Theoretical and Observed Acoustic-Gravity Waves from Explosive Sources in the Atmosphere[1]

DAVID G. HARKRIDER

California Institute of Technology, Pasadena

Abstract. A matrix formulation is used to derive the pressure variation for acoustic-gravity waves from an explosive source in an atmosphere modeled by a large number of isothermal layers. Comparison of theoretical and observed barograms from large thermonuclear explosions leads to the following conclusions: (1) The major features on the barogram can be explained by the superposition of four modes, (2) different parts of the vertical temperature structure of the atmosphere control the relative excitation of these modes, (3) a scaled point source is sufficient to model thermonuclear explosions, (4) the observed shift in dominance of certain frequencies with yield and altitude can be explained by means of the empirical scaling laws derived from the direct wave near the explosion, and (5) out to 50° from the source, the observed variation of amplitude with distance can be accounted for by geometrical spreading over a spherical surface.

Introduction. During the past few years, a large number of thermonuclear bombs have been exploded in the atmosphere. These events have given geophysicists a controlled experiment with which to test the theories of pulse propagation in a complex wave guide. The value of the experiment is enhanced by the fact that the 'megaton'-class explosions were large enough to excite long atmospheric waves which were recorded by a world-wide net of sensitive barographs [*Yamomoto,* 1956, 1957; *Hunt et al.,* 1960; *Rose et al.,* 1961; *Carpenter et al.,* 1961; *Donn and Ewing,* 1962*a, b*; *Wexler and Hass,* 1962].

Early theoretical studies [*Scorer,* 1950; *Pekeris,* 1948; *Yamomoto,* 1957; *Hunt et al.,* 1960] were of limited use in analyzing these barograms because of their oversimplified atmospheric models.

With the advent of high-speed computers it became possible to obtain numerical solutions for more realistic atmospheric models. Numerical solutions of the problem have been formulated by two different approaches. The first study with a complex temperature model was made by *Weston* [1960, 1961*a, b, c*]. He formulated the inhomogeneous problem of an explosive source in an atmosphere with a continuous vertical temperature distribution. The problem of determining the eigenfrequencies and eigenfunctions was reduced to the evaluation of a second-order differential equation with coefficients that vary with altitude.

Papers by *Press and Harkrider* [1962] and *Pfeffer and Zarichny* [1962] used a matrix formulation suggested by *Haskell* [1953] in which the vertical temperature of the atmosphere was represented by a large number of isothermal layers. The resultant multilayered matrix formulation is particularly suited for programming on a digital computer.

These papers presented results for the homogeneous problem of wave propagation in which the atmosphere is considered a two-dimensional wave guide without a source. Phase and group velocity dispersion curves and vertical pressure distributions were numerically evaluated for a number of modes and discussed in terms of the different models of atmospheric structure. The results of *Press and Harkrider* [1962] and *Pfeffer and Zarichny* [1962] differed somewhat because the latter authors terminated their atmosphere model at a lower altitude. Later work with a more complete model [*Pfeffer and Zarichny,* 1963] gives results which agree with those of Press and Harkrider and contains a wider variety of atmospheric models.

In this paper the homogeneous theory of Press and Harkrider is extended to include the effect of an explosive source at various altitudes in the atmosphere. We first represent the com-

[1] Contribution 1283, Division of Geological Sciences, California Institute of Technology, Pasadena.

plex vertical temperature structure of the atmosphere by a large number of horizontally stratified isothermal layers. In one of the layers, we place a point source. The strength of the source in the frequency domain is scaled so that the pressure variation with time of the direct wave near the source is in agreement with the observations near actual nuclear detonations.

After the far-field term of the plane multilayered solution is obtained, it is approximately corrected for curvature in order to represent the spectral amplitude and phase of acoustic-gravity waves traveling over a spherical earth. The inhomogeneous theory, i.e., source inclusion, then makes it possible to calculate the effect of source altitude and yield on the spectral amplitude of various modes. With the inhomogeneous theory and the known response of the observing barograph we are able to calculate theoretical barograms in the time domain. These theoretical barograms are compared with actual barograms recorded at Pasadena for the 1961 Soviet nuclear atmospheric test series.

Some of the early studies also included the effect of sources [*Pekeris*, 1948; *Hunt et al.*, 1960]. In these studies the effect of source altitude was not investigated, since they were concerned with surface explosions. The recent papers by Weston mentioned above included the effect of source height. His technique is limited by the difficulty in obtaining from the available nuclear test data the actual excess pressures and normal velocities on a surface enclosing an explosion. This difficulty is overcome in this paper by the use of a closed-form expression for the source model. The form of the source term is such that it may readily be scaled to represent the observed pressure-time variation of the direct wave at locations near the source.

Pfeffer and Zarichny [1963] also present a theoretical barogram for a point source at an altitude of 2 km and a distance of 6650 km. The details or references for obtaining the relative excitation function were not given, and no attempt was made to calculate the absolute pressure for a given yield and altitude.

Symbols.

p, excess pressure.
r, horizontal cylindrical coordinate.
z, vertical cylindrical coordinate or altitude.
h, square of the vertical scale factor.
α, acoustic velocity.
$\gamma = C_p/C_v$, specific heat ratio.
g, gravity field strength.
ω, angular frequency.
σ_2, Brunt cutoff frequency.
t, time.
D, source altitude.
s, subscript denoting source medium.
$\langle p_{s0} \rangle$, excess pressure of source in frequency domain.
2λ, exponential decay factor of density with altitude in isothermal layer.
$i\kappa_s$, horizontal wave number of direct source wave.
$f(\omega, a_s)$, source scaling factor.
a_s, scaling distance for direct source wave.
J_0, Bessel function of zero order.
$[p_{s0}]$, excess pressure of source in time domain.
p_{as}, peak excess pressure at a_s.
t_{as}, arrival time of peak excess pressure at a_s.
T_{+as}, duration of the positive phase at a_s.
$b_s = (T_{+as})^{-1}$.
τ, time after some fiducial time.
$i\chi_s$, vertical wave number of direct source wave.
σ_1, acoustic cutoff.
a_0, standard scaling distance.
ξ, distance scale factor.
W, yield.
p^0, ambient pressure.
ρ^0, ambient density.
ρ, density perturbation.
R^*, universal gas constant.
M_0, molecular weight at ground.
$R = R^*/M_0$.
K^*, real kinetic temperature in degrees Kelvin.
$K = (M_0/M)K^*$, molecular scale temperature.
m, subscript denoting mth layer constants.
$kr_{\alpha m}$, vertical air wave number in layer m.
k, horizontal wave number.
w_m, vertical particle velocity perturbation in layer m.
p_{Pm}, excess pressure at upper interface of layer m.
z_m, the altitude at the top of layer m.
$d_m = z_m - z_{m-1}$, thickness of layer m.
$\mathfrak{A}_m$, air wave matrix for layer m.
Δ_m', propagation coefficient of ascending wave in layer m.
Δ_m'', propagation coefficient of descending wave in layer m.
S_0, source coefficient in the frequency–wave number domain.
n, the number of layers including half-space.

A, product matrix of layer matrices from 1 to $n-1$.
A_{s1}, product matrix of layer matrices from 1 to $s1$.
A^{s2}, product matrix of layer matrices from $s2$ to n.
p_0, excess pressure at the earth's surface.
δw_s, discontinuity in vertical particle velocity integrand at source.
δp_{ps}, discontinuity in pressure integrand at source.
X, vector element defined by (33).
Y, vector element defined by (33).
E_n^{-1}, matrix defined by (37).
b_{1n}, matrix element defined by (38).
b_{2n}, matrix element defined by (38).
$c = \omega/k$, horizontal phase velocity.
$N_A^{(1)}$, integrand numerator factor defined by (41).
F_A, integrand denominator defined by (41).
$N_A^{(2)}$, integrand numerator factor defined by (43).
$\langle\ \rangle$, designates frequency domain quantity.
j, subscript denotes roots of $F_A = 0$.
$\{\ \}_{Aj}$, designates residue contribution of integral solution.
$[\ ]_{Hj}$, homogeneous ratio evaluated at jth root of $F_A = 0$.
$H_0^{(2)}$, Hankel function of zero order.
a_e, radius of the earth.
θ, spherical colatitude angle.
ν, separation constant.
P_ν, Q_ν, Legendre functions.
$\mathfrak{R}$, amplitude of barograph response.
φ_I, phase of barograph response.
ω_F, natural frequency of the float transducer.
ϵ_F, damping constant of the float transducer.
ω_G, natural frequency of the galvanometer.
ϵ_G, damping constant of the galvanometer.
σ, coupling factor.
$[\ ]_{Aj}$, denotes time domain expression.
I_1, defined by (67).
I_2, defined by (67).
$\mathfrak{F}_A^{(1)}$, defined by (67).
$\mathfrak{F}_A^{(2)}$, defined by (67).
$\mathbf{A}_{Aj}$, amplitude response of surface source and receiver; defined by (67).
τ_A, defined by (67).
θ_s, phase of source time function.
τ_A', defined by (67).
τ_X, defined by (67).
U, horizontal group velocity.

Theoretical explosive-source model. The partial differential equation governing the excess pressure p in an isothermal gravitating atmosphere can be given in cylindrical coordinates by

$$\frac{1}{r}\frac{\partial}{\partial r}\left(r\frac{\partial p}{\partial r}\right) + \frac{1}{h}\left(\frac{\partial^2 p}{\partial z^2} + \frac{\gamma g}{\alpha^2}\frac{\partial p}{\partial z} + \frac{\omega^2}{\alpha^2}p\right) = 0 \qquad (1)$$

where

$$h = 1 - [(\gamma - 1)/\omega^2\alpha^2]g^2 = 1 - \sigma_2^2/\omega^2$$

and a time dependence of $e^{i\omega t}$ has been assumed. The derivation of (1) closely parallels the derivation given by *Lamb* [1945] and *Pekeris* [1948] for the first time derivative of the dilatation and will not be given here.

As a source model for an atmospheric nuclear blast, we use an azimuthally symmetric, simple point source located in layer s at an altitude D. This point source or Green's function, located at $r = 0$ and $z = D$, is here defined as the particular solution of the elementary inhomogeneous form of (1), or

$$\frac{1}{r}\frac{\partial}{\partial r}\left(r\frac{\partial p_s}{\partial r}\right) + \frac{1}{h_s}\left(\frac{\partial^2 p_s}{\partial z^2} + \frac{\gamma g_s}{\alpha_s^2}\frac{\partial p_s}{\partial z} + \frac{\omega^2}{\alpha_s^2}p_s\right) = \frac{\delta(r)}{r}\delta(z - D)e^{i\omega t} \qquad (2)$$

The solution of (2) is given by

$$\langle p_{s0}\rangle = -\frac{h_s^{1/2}}{2}e^{-\lambda_s(z-D)} \cdot \frac{e^{-\kappa_s[r^2+h_s(z-D)^2]^{1/2}}}{[r^2 + h_s(z-D)^2]^{1/2}}e^{i\omega t} \qquad (3)$$

where

$$\kappa_s^2 = (\alpha_s^2\lambda_s^2 - \omega^2)/h_s\alpha_s^2 \quad \lambda_s = \gamma g_s/2\alpha_s^2$$

It is easy to verify by direct substitution that the Green's function (3) is a solution of the homogeneous equation (1) for all (r, z) except at the point $(0, D)$. Also, if we let $g = 0$, the Green's function reduces to the well-known point source for outgoing spherical pressure waves in an acoustic medium.

$$\langle p\rangle = -(1/2R)e^{i\omega(t-R/\alpha)}$$

where $R = [r^2 + (z - D)^2]^{1/2}$.

We now insert $f(\omega, a_s)$ in (3), so that after integrating (3) over ω we have at a distance a_s directly below the source, the observed excess pressure-time variation [*Glasstone*, 1962].

$$[p_{s0}(0, D - a_s; t)] = \begin{cases} p_{as}(1 - \tau/T_{+as})e^{-\tau/T_{+as}} & \text{for } \tau \geq 0 \\ 0 & \text{for } \tau < 0 \end{cases} \quad (4)$$

where $\tau = t - t_{as}$. Applying a Fourier transform to (4)

$$\int_{-\infty}^{\infty} [p_{s0}(0, D - a_s; t)]e^{-i\omega t}\, dt = p_{as}e^{-i\omega t_{as}} \frac{i\omega}{(i\omega + 1/T_{+as})^2} \quad (5)$$

and equating the result to (3), evaluated at $(0, D - a_s)$ with the $e^{i\omega t}$ excluded, yields

$$f(\omega, a_s) = -2p_{as}e^{(\chi_s - \lambda_s)a_s}e^{-i\omega t_{as}} \cdot \frac{a_s i\omega}{(b_s + i\omega)^2} \quad (6)$$

where $b_s = 1/T_{+as}$ and $\chi_s^2 = \kappa_s^2 h_s$. Thus, for an explosion source, we have

$$\langle p_{s0} \rangle = h_s^{1/2} p_{as}e^{(\chi_s - \lambda_s)}e^{-\lambda_s(z-D)}e^{-i\omega t_{as}} \cdot \frac{a_s i\omega}{(b_s + i\omega)^2} \frac{e^{-\kappa_s[r^2 + h_s(z-D)^2]^{1/2}}}{[r^2 + h_s(z - D)^2]^{1/2}} e^{i\omega t} \quad (7)$$

We note that κ_s has four branch points located at $\omega = \pm\sigma_1$ and $\pm\sigma_2$, and $h_s^{1/2}$ has two branch points located at $\omega = \pm\sigma_2$, where $\sigma_1^2 = \gamma^2 g_s^2/4\ \alpha_s^2$ and $\sigma_2^2 = (\gamma - 1)g_s^2/\alpha_s^2$. In order that the integration of (7) over ω be convergent for all reasonable (r, z) outside of a_s, we require that for

$$\sigma_2 > \omega > -\sigma_2$$

$$\kappa_s = i(\omega/\alpha_s)[(\sigma_1^2 - \omega^2)/(\sigma_2^2 - \omega^2)]^{1/2}$$

and

$$h_s^{1/2} = -i(\sigma_2^2 - \omega^2)^{1/2}/\omega$$

for

$$\sigma_1 > \omega > \sigma_2 \quad \text{and} \quad -\sigma_1 < \omega < -\sigma_2 \quad (8)$$

$$\kappa_s = (|\omega|/\alpha_s)[(\sigma_1^2 - \omega^2)/(\omega^2 - \sigma_2^2)]^{1/2}$$

and

$$h_s^{1/2} = (\omega^2 - \sigma_2^2)^{1/2}/|\omega|$$

for

$$\omega > \sigma_1 \quad \text{and} \quad -\sigma_1 > \omega$$

$$\kappa_s = i(\omega/\alpha_s)[(\omega^2 - \sigma_1^2)/(\omega^2 - \sigma_2^2)]^{1/2}$$

and

$$h_s^{1/2} = (\omega^2 - \sigma_2^2)^{1/2}/|\omega|$$

where

$$\sigma_1^2 > \sigma_2^2$$

for $\gamma > 1$. Although not shown here, the above criteria can be obtained by shifting paths of integration in the complex ω plane arbitrarily close to the real axis under the condition that $\mathrm{Re}\,(\kappa_s) > 0$ and $\mathrm{Re}(h_s^{1/2}) > 0$.

The condition that $\mathrm{Re}(\kappa_s) > 0$ and $\mathrm{Re}(h_s^{1/2}) > 0$ enables us to write (7) as the following expression [*Erdelyi et al.*, 1954]:

$$\langle p_{s0} \rangle = h_s p_{as}e^{(\chi_s - \lambda_s)a_s}e^{-\lambda_s(z-D)}e^{-i\omega t_{as}} a_s i\omega \cdot \int_0^{\infty} \frac{e^{-ikr_{\alpha s}|z-D|}}{ikr_{\alpha s}} J_0(kr)k\, dke^{i\omega t} \quad (9)$$

where

$$(kr_{\alpha s})^2 = \omega^2/\alpha_s^2 - h_s k^2 - \gamma^2 g_s^2/4\alpha_s^4 \quad (10)$$

This form will be used as our source term in the matrix formulation because, as we shall see, its integrand is expressed in the solutions of the homogeneous excess-pressure equation.

Instead of inserting a different p_{as}, a_s, t_{as}, and T_{+as} for different yields and altitudes in order to synthesize a barogram, we use the measurements from a 'standard' bomb size of 1 kiloton at a p_{a0} such that a_0 is in the linear region; then, keeping p_{a0} fixed, we scale the other parameters to explosives under different conditions by means of the empirical scale factors given by *Glasstone* [1962]. For a given excess pressure, the distance from the blast at which it is found is given by the distance scale factor

$$\xi = (W_s p_0^0/p_s^0)^{1/3} \quad (11)$$

For the time measurements t_{as} and T_{+as} at this new distance, we use ξ and in addition a velocity ratio, since the standard quantities are given at surface or sea-level velocities. According to these scaling laws, the appropriate bomb character-

istics for yields and altitudes other than the reference or 'standard' bomb are

$$a_s = \xi a_0 \quad t_{as} = \xi \frac{\alpha_0}{\alpha_s} t_{a0} \quad T_{+as} = \xi \frac{\alpha_0}{\alpha_s} T_{+a0} \quad (12)$$

where

$$\xi = (W_s p_0^0/p_s^0)^{1/3} = (W_s \rho_0^0 \alpha_0^2/\rho_s^0 \alpha_s^2)^{1/3} \quad (13)$$

since, by the equation of state, $p^0 = RK^0\rho^0$ and $\alpha^2 = \gamma RK^0 = \gamma p^0/\rho^0$.

Matrix formulation and solution for the explosive source in a horizontally stratified atmosphere. For an isothermal or constant velocity layer m in a horizontally stratified atmosphere not containing the source, the equation for excess pressure is given by (1):

$$\frac{1}{r}\frac{\partial}{\partial r}\left(r\frac{\partial p_m}{\partial r}\right) + \frac{1}{h_m}\left(\frac{\partial^2 p_m}{\partial z^2} + \frac{\gamma g_m}{\alpha_m^2}\frac{\partial p_m}{\partial z} + \frac{\omega^2}{\alpha_m^2} p_m\right) = 0 \quad (14)$$

If the radial or r dependence of p_m is given by $J_0(kr)$, (14) reduces to

$$\frac{\partial^2 p_m}{\partial z^2} + \gamma \frac{g_m}{\alpha_m^2}\frac{\partial p_m}{\partial z} + \left(\frac{\omega^2}{\alpha_m^2} - k_m k^2\right)p_m = 0 \quad (15)$$

Making use of *Press and Harkrider*'s [1962] first three equations we can express the vertical velocity perturbation as

$$w_m = \frac{i}{\omega \rho_m^0(z) h_m}\left(\frac{\partial p_m}{\partial z} + \frac{g_m}{\alpha_m^2} p_m\right) \quad (16)$$

As in *Press and Harkrider* [1962], the boundary conditions are continuity of vertical particle velocity and total pressure across the disturbed interfaces. Since the equations of motion were linearized under the assumption of small motion, we retain only first-order terms. With this assumption we find that the change in total pressure at an interface which is displaced a vertical distance, $-iw/\omega$, from its static equilibrium position is given by

$$p_{Pm} = p_m - \frac{g_m}{\omega^2 h_m}\left(\frac{\partial p_m}{\partial z} + \frac{g_m}{\alpha_m^2} p_m\right) \quad (17)$$

Therefore, at the layer interfaces we require

$$w_m(z_{m-1}) = w_{m-1}(z_{m-1}) \quad (18)$$

$$p_{Pm}(z_{m-1}) = p_{Pm-1}(z_{m-1}) \quad (19)$$

in order to guarantee continuity of vertical particle velocity and total pressure.

The general solution of (14) is given by

$$p_m = e^{-\lambda m z}[\Delta_m' e^{-ikr\alpha_m z} + \Delta_m'' e^{ikr\alpha_m z}]J_0(kr)e^{i\omega t} \quad (20)$$

Substituting (20) in (16) and (17), evaluating at the top, z_m, and bottom, z_{m-1}, of layer m, and eliminating the propagation coefficients Δ_m' and Δ_m'', we obtain the following matrix relation:

$$\begin{bmatrix} w_m(z_m) \\ p_{Pm}(z_m) \end{bmatrix} = \mathfrak{A}_m \begin{bmatrix} w_m(z_{m-1}) \\ p_{Pm}(z_{m-1}) \end{bmatrix} \quad (21)$$

where the elements of the $\mathfrak{A}_m$ matrix are given by *Press and Harkrider*'s [1962] equations 12.

For layer s, which contains the source, we add a source term of the form

$$p_{s0}(z) = S_0 e^{-\lambda_s(z-D)} e^{-ikr\alpha_s|z-D|} J_0(kr)e^{i\omega t} \quad (22)$$

where S_0 is not a function of r or z, so that we now have

$$p_s(z) = e^{-\lambda_s z}[\Delta_s' e^{-ikr\alpha_s z} + \Delta_s'' e^{ikr\alpha_s z} + S_0 e^{\lambda_s D} e^{-ikr\alpha_s|z-D|}]J_0(kr)e^{i\omega t} \quad (23)$$

Decomposing layer s into two layers, $s2$ and $s1$, with the same temperature and g, we can write (23) as

$$p_{s2}(z) = e^{-\lambda_s z}\{[\Delta_s' + S_0 e^{(\lambda_s + ikr\alpha_s)D}]e^{-ikr\alpha_s z} + \Delta_s'' e^{ikr\alpha_s z}\}J_0(kr)e^{i\omega t} \quad (24)$$

for $z_s \geq z \geq D$ and

$$p_{s1}(z) = e^{-\lambda_s z}\{\Delta_s' e^{-ikr\alpha_s z} + [\Delta_s'' + S_0 e^{(\lambda_s - ikr\alpha_s)D}]e^{ikr\alpha_s z}\}J_0(kr)e^{i\omega t} \quad (25)$$

for $D \geq z \geq z_{s-1}$

Evaluating (24) and (25) at the tops and bottoms of their respective sublayers and eliminating the propagation coefficients, we see that for layers $s2$ and $s1$ we have the same matrix relation as is given in (21), with the m subscripts replaced by $s2$ and $s1$, respectively. Also, it can be shown that the matrix product

$$\mathfrak{A}_{s2}\mathfrak{A}_{s1} = \mathfrak{A}_s \quad (26)$$

where $\mathfrak{A}_s$ is the layer matrix for layer s if no source is present.

For all interfaces except the interface between

layers $s2$ and $s1$, we have continuity of w and p_P. Using this continuity and the matrix relation (21), we get

$$\begin{bmatrix} w_{n-1}(z_{n-1}) \\ p_{Pn-1}(z_{n-1}) \end{bmatrix} = A^{s2} \begin{bmatrix} w_{s2}(D) \\ p_{Ps2}(D) \end{bmatrix} \tag{27}$$

and

$$\begin{bmatrix} w_{s1}(D) \\ p_{Ps1}(D) \end{bmatrix} = A_{s1} \begin{bmatrix} w_1(0) \\ p_{P1}(0) \end{bmatrix} \tag{28}$$

where $A^{s2} = \mathfrak{A}_{n-1} \cdots \mathfrak{A}_{s2}$ and $A_{s1} = \mathfrak{A}_{s1} \cdots \mathfrak{A}_1$. At $z = 0$, layer 1 is in contact with a flat rigid boundary where we require $w_1(0) = 0$, and thus $p_{P1}(0) = p_1(0) \equiv p_0$. Equation 28 then reduces to

$$\begin{bmatrix} w_{s1}(D) \\ p_{Ps1}(D) \end{bmatrix} = A_{s1} \begin{bmatrix} 0 \\ p_0 \end{bmatrix} \tag{29}$$

Since $\partial p_{s0}/\partial z$ is discontinuous across $z = D$, we have, from (24) and (25), substituted in (16) and (17) the following relations:

$$\begin{aligned} p_{s2}(D) - p_{s1}(D) &= 0 \\ w_{s2}(D) - w_{s1}(D) &= \frac{i}{\omega \rho_s{}^0(D) h_s} \left[\frac{\partial p_{s2}(D)}{\partial z} - \frac{\partial p_{s1}(D)}{\partial z} \right] \\ p_{Ps2}(D) - p_{Ps1}(D) &= -\frac{g_s}{\omega^2 h_s} \left[\frac{\partial p_{s2}(D)}{\partial z} - \frac{\partial p_{s1}(D)}{\partial z} \right] \end{aligned} \tag{30}$$

and

$$\left[\frac{\partial p_{s2}(D)}{\partial z} - \frac{\partial p_{s1}(D)}{\partial z} \right] = -i2kr_{\alpha s} S_0 J_0(kr) e^{i\omega t}$$

where the partial derivatives with respect to z are evaluated at D by letting z approach D from their respective layers. From (30) we obtain the vector relation

$$\begin{bmatrix} w_{s2}(D) \\ p_{Ps2}(D) \end{bmatrix} = \begin{bmatrix} w_{s1}(D) \\ p_{Ps1}(D) \end{bmatrix} + \begin{bmatrix} \delta w_s \\ \delta p_{Ps} \end{bmatrix} \tag{31}$$

where

$$\begin{aligned} \delta w_s &= \frac{2kr_{\alpha s} S_0}{\omega h_s \rho_s{}^0(D)} J_0(kr) e^{i\omega t} \\ \delta p_{Ps} &= \frac{i g_s \rho_s{}^0(D)}{\omega} \delta w_s \end{aligned} \tag{32}$$

We now define X and Y by the matrix operation

$$\begin{bmatrix} X \\ Y \end{bmatrix} = A_{s1}{}^{-1} \begin{bmatrix} w_{s2}(D) \\ p_{Ps2}(D) \end{bmatrix} \tag{33}$$

Multiplying (31) by $A_{s1}{}^{-1}$, and using (33) and (29), we have

$$\begin{bmatrix} X \\ Y \end{bmatrix} = \begin{bmatrix} 0 \\ p_0 \end{bmatrix} + A_{s1}{}^{-1} \begin{bmatrix} \delta w_s \\ \delta p_{Ps} \end{bmatrix} \tag{34}$$

or

$$\begin{aligned} X &= (A_{s1}{}^{-1})_{11} \delta w_s + (A_{s1}{}^{-1})_{12} \delta p_{Ps} \\ p_0 &= Y - [(A_{s1}{}^{-1})_{21} \delta w_s + (A_{s1}{}^{-1})_{22} \delta p_{Ps}] \end{aligned} \tag{35}$$

For the case of an atmosphere bounded by an isothermal half-space, we require that the nth layer propagation coefficient $\Delta_n'' = 0$. For (ω, k) such that $(kr_{\alpha n})^2 > 0$, this is equivalent to requiring that there be no radiation from infinity into the wave guide. For (ω, k) such that $(kr_{\alpha n})^2 < 0$, this condition guarantees that the kinetic energy integrated over a column of atmosphere be finite.

Setting $\Delta_n'' = 0$ in equations for $w_n(z)$ and $p_{Pn}(z)$ evaluated at z_{n-1}, we find that

$$\begin{bmatrix} \Delta_n' \\ \Delta_n' \end{bmatrix} = E_n{}^{-1} \begin{bmatrix} w_{n-1}(z_{n-1}) \\ p_{Pn-1}(z_{n-1}) \end{bmatrix} \tag{36}$$

and the matrix $E_n{}^{-1}$ is given by

$$E_n{}^{-1} = \begin{bmatrix} (1/b_{1n}) & 0 \\ 0 & (1/b_{2n}) \end{bmatrix} \tag{37}$$

where

$$\begin{aligned} b_{1n} &= \frac{e^{\lambda_n z_{n-1}}}{\delta_n} e^{-ikr_{\alpha n} z_{n-1}} (kc)^2 \cdot \{ g_n(\alpha_n{}^2/c^2 - \gamma/2) - i\alpha_n{}^2 (kr_{\alpha n}) \} J_0(kr) e^{i\omega t} \\ b_{2n} &= i \frac{e^{\lambda_n z_{n-1}}}{\delta_n} e^{-ikr_{\alpha n} z_{n-1}} (kc)^2 \cdot \frac{\rho_n{}^0(z_{n-1})}{(kc)^3} \alpha_n{}^2 \delta_n J_0(kr) e^{i\omega t} \end{aligned} \tag{38}$$

$$c = \omega/k$$

Defining the matrix A by the matrix product

$$A = A^{s2}A_{s1} = \mathfrak{A}_{n-1} \cdots \mathfrak{A}_{s2}\mathfrak{A}_{s1} \cdots \mathfrak{A}_1$$
$$= \mathfrak{A}_{n-1} \cdots \mathfrak{A}_s \cdots \mathfrak{A}_1$$

we obtain from (36), (27), and (33)

$$\begin{bmatrix} \Delta_n' \\ \Delta_n' \end{bmatrix} = E_n^{-1} A \begin{bmatrix} X \\ Y \end{bmatrix} \tag{39}$$

Finally, eliminating Δ_n' from (39), we have

$$Y = i(N_A^{(1)}/F_A)X \tag{40}$$

where

$$N_A^{(1)} = A_{11} - (b_{1n}/b_{2n}^*)A_{21}^*$$
$$F_A = A_{12}^* + (b_{1n}/b_{2n}^*)A_{22} \tag{41}$$
$$iA_{jk}^* = A_{jk} \quad \text{and} \quad ib_{2n}^* = b_{2n}$$

Substituting (40) in (35) yields

$$p_0 = i\delta w_s \frac{N_A^{(1)}N_A^{(2)}}{F_A} \tag{42}$$

where

$$N_A^{(2)} = \left[(A_{s1}^{-1})_{11} + \frac{\delta p_{Ps}}{\delta w_s}(A_{s1}^{-1})_{12}\right]$$
$$- \frac{F_A}{N_A^{(1)}}\left[(A_{s1}^{-1})_{21} + \frac{\delta p_{Ps}}{\delta w_s}(A_{s1}^{-1})_{22}\right] \tag{43}$$

From *Press and Harkrider* [1962] we know that the determinant of the individual layer matrix is equal to unity; therefore, the determinant of any matrix product of these layer matrices is also equal to unity. Therefore, the inverse of A_{s1} is given by

$$A_{s1}^{-1} = \begin{bmatrix} (A_{s1})_{22} & -(A_{s1})_{12} \\ -(A_{s1})_{21} & (A_{s1})_{11} \end{bmatrix} \tag{44}$$

Substituting this result in (43) yields

$$N_A^{(2)} = \left[(A_{s1})_{22} - \frac{\delta p_{Ps}}{\delta w_s}(A_{s1})_{12}\right]$$
$$+ \frac{F_A}{N_A^{(1)}}\left[(A_{s1})_{21} - \frac{\delta p_{Ps}}{\delta w_s}(A_{s1})_{11}\right] \tag{45}$$

Using (32), the definition of p_p, and (29), we get

$$N_A^{(2)} = \frac{p_{s1}(D)}{p_0}$$
$$+ iF_A[(A_{s1})_{21}^* - g_s\rho_s^0(D)(A_{s1})_{11}] \tag{46}$$

Performing an integration over k, where

$$\langle p_m \rangle = \int_0^\infty p_m\, dk \quad \langle w_m \rangle = \int_0^\infty w_m\, dk$$
$$\langle p_{Pm} \rangle = \int_0^\infty p_{Pm}\, dk \tag{47}$$

and letting

$$S_0 = p_{as}\omega a_s e^{(\chi_s - \lambda_s)a_s} \frac{h_s}{(b_s + i\omega)^2} \frac{e^{i\omega t_{as}}}{r_{as}} \tag{48}$$

in order that $p_{s0} = \int_0^\infty p_{s0}dk$ be equal to (9), we have from (32)

$$\delta w_s = \frac{2k}{\rho_s^0(D)} a_s p_{as} \frac{e^{(\chi_s - \lambda_s)a_s}}{(b_s + i\omega)^2}$$
$$\cdot J_0(kr)e^{i\omega(t - t_{as})} \tag{49}$$

and

$$\langle p_0 \rangle = ia_s \frac{p_{as}}{\rho_s^0(D)} \frac{e^{(\chi_s - \lambda_s)a_s}}{(b_s + i\omega)^2} e^{i\omega(t - t_{as})} 2$$
$$\cdot \int_0^\infty \frac{N_A^{(1)}N_A^{(2)}}{F_A} J_0(kr)k\, dk \tag{50}$$

In this paper we are interested only in the waves which are $O(r^{-1/2})$. These waves are given by the residue contribution of (50) due to the zeros of F_A. Evaluating (50) for the residue contribution, we obtain for each mode or k_j root, ω fixed, of $F_A = 0$

$$\{p_0\}_{Aj} = 2\pi \frac{a_s p_{as}}{\rho_s^0(D)} \frac{e^{(\chi_s - \lambda_s)a_s}}{(b_s + i\omega)^2} k_j$$
$$\cdot \frac{N_{Aj}^{(1)}N_{Aj}^{(2)}}{\left(\frac{\partial F_A}{\partial k}\right)_{\omega,j}} H_0^{(2)}(k,r)e^{i\omega(t - t_{as})} \tag{51}$$

where $(\partial F_A/\partial k)_{\omega,j}$, $N_A^{(1)}$, and $N_{Aj}^{(2)}$ are evaluated at (ω, k_j) so that $F_A(\omega, k) = 0$. $F_A = 0$ is the period equation given by *Press and Harkrider* [1962]. Roots, dispersion curves, and the homogeneous velocity and pressure ratios at altitude for various temperature models of the atmosphere, along with a discussion of the 'cutoff' region, can be found in this reference.

At $F_A(\omega, k_j) = 0$, by (46),

$$N_{Aj}^{(2)} = \frac{p_{s1(D)}}{p_0} \tag{52}$$

and, since the determinant of product matrix is unity, that is

$$|A| \equiv A_{11}A_{22} + A_{12}^*A_{21}^* = 1$$

and since

$$F_A \equiv A_{12}^* + \frac{b_{1n}}{b_{2n}^*} A_{22} = 0$$

we have

$$N_{A_i}^{(1)} = \frac{1}{A_{22}} \tag{53}$$

Evaluating the residue contributions of the integral representations for $\langle w_{s1}(D)\rangle$, $\langle p_{Ps1}(D)\rangle$, $\langle p_{s1}(D)\rangle$, $\langle w_{s2}(D)\rangle$, $\langle p_{Ps2}(D)\rangle$, and $\langle p_{s2}(D)\rangle$ by using (27) and (31), we find that

$$\begin{aligned} \{w_{s1}(D)\}_{A_i} &= (A_{s1})_{12}\{p_0\}_{Ai} \\ \{p_{Ps1}(D)\}_{Ai} &= (A_{s1})_{22}\{p_0\}_{Ai} \end{aligned} \tag{54}$$

$$\{p_{s1}(D)\}_{A_i} = \left[(A_{s1})_{22} + \frac{\rho_s^0(D)}{\omega} g_s(A_{s1})_{12}^*\right]\{p_0\}_{Ai}$$

$$\begin{aligned} \{w_{s2}(D)\}_{Ai} &= \{w_{s1}(D)\}_{Ai} \\ \{p_{Ps2}(D)\}_{A_i} &= \{p_{Ps1}(D)\}_{Ai} \\ \{p_{s2}(D)\}_{Ai} &= \{p_{s1}(D)\}_{Ai} \end{aligned} \tag{55}$$

and thus there is no discontinuity across the source plane, $z = D$, for the residue contributions. From (55) we see that

$$\{w_m(z)\}_{A_i}^* = [A_m(z)]_{12}^*\{p_0\}_{Ai} \equiv \left[\frac{w_m^*(z)}{p_0}\right]_{Hi}\{p_0\}_{Ai}$$

$$\{p_{Pm}(z)\}_{Ai} = [A_m(z)]_{22}\{p_0\}_{Ai} \equiv \left[\frac{p_{Pm}(z)}{p_0}\right]_{H_i}\{p_0\}_{Ai} \tag{56}$$

$$\{p_m(z)\}_{Ai} = \{[A_m(z)]_{22} + \frac{\rho_m^0(z)\, g_m}{\omega}[A_m(z)]_{12}^*\} \cdot \{p_0\}_{A_i} \equiv \left[\frac{p_m(z)}{p_0}\right]_{H_i}\{p_0\}_{A_i}$$

is true for all m above and below the source, where

$$A_m(z) = \mathfrak{A}_m(z)\mathfrak{A}_{m-1} \cdots \mathfrak{A}_1$$

and $\mathfrak{A}_m(z)$ is the layer matrix for a sublayer in layer m of thickness $d_m(z) = z - z_{m-1}$.

Rewriting (51), using (52), (53) and the definitions in (56), we obtain for the residue contribution for excess pressure at the surface of a horizontally stratified atmosphere

$$\{p_0\}_{Ai} = 2\pi \frac{a_s p_{as}}{\rho_s^0(D)} \frac{e^{(\chi_s - \lambda_s)a_s}}{(b_s + i\omega)^2} k_i \cdot \frac{\left[\frac{p_s(D)}{p_0}\right]_{Hi}}{\left[\frac{p_{n-1}}{p_0}\right]_{H_i}\left(\frac{\partial F_A}{\partial k}\right)_{\omega,i}} H_0^{(2)}(k_i r) e^{i\omega(t - t_{as})} \tag{57}$$

where

$$\left[\frac{p_{n-1}}{p_0}\right]_{H_i} \equiv \left[\frac{p_{n-1}(z_{n-1})}{p_0}\right]_{Hi}$$

Approximate curvature correction. It has been shown by *Weston* [1961] that a good approximation to the equation for excess pressure in an isothermal gravitating spherical layer, assuming that the radial dimension of the atmosphere is small in comparison with the earth's radius, a_e, can be given for longitudinal symmetry by

$$\frac{1}{\sin\theta}\frac{\partial}{\partial\theta}\left(\sin\theta\frac{\partial p_m}{\partial\theta}\right) + \nu(\nu+1)p_m = 0 \tag{58}$$

and

$$\frac{\partial^2 p_m}{\partial z^2} + \frac{\gamma g_m}{\alpha_m^2}\frac{\partial p_m}{\partial z} + \left(\frac{\omega^2}{\alpha_m^2} - h_m k^2\right)p_m = 0 \tag{59}$$

where z is the radial coordinate, θ is the colatitude, and

$$k^2 a_e^2 = \nu(\nu+1) \tag{60}$$

To this approximation the θ dependence of p_m is given by the Legendre functions $P_\nu(\cos\theta)$ and $Q_\nu(\cos\theta)$, and the radial dependence is determined by the same differential equation as (15), which governed the vertical dependence of p_m for the horizontal layer. Also, the approximate radial boundary conditions across spherical layers are the same as for the horizontal layers. Thus we have the same relation for the spherically layered atmosphere as (42), with the $J_0(kr)$ dependence of δw_s replaced by some linear combination of $P_\nu(\cos\theta)$ and $Q_\nu(\cos\theta)$.

Now, near the source, the residue contribution (57) should be valid for k_i large, i.e., small horizontal wavelengths. Thus for an approximate curvature correction to (57), valid for large

$k_j a_e$, we use an asymptotic expansion, valid for large ν, of the Legendre functions which reduces to $H_0^{(2)}(k_j r)$ near the source, i.e., θ small. Such an expansion was given by *Szegö* [1933].

$$P_\nu(\cos\theta) + i(2/\pi)Q_\nu(\cos\theta) \approx (\theta/\sin\theta)^{1/2} H_0^{(2)}[(\nu + \tfrac{1}{2})\theta] \qquad (61)$$

For ν large, $k_j a_e \approx \nu + \frac{1}{2}$ and (61) yields

$$P_\nu(\cos\theta) + i(2/\pi)Q_\nu(\cos\theta) \approx (r/a_e \sin\theta)^{1/2} H_0^{(2)}(k_j r)$$

where r is the distance from the source measured on the surface of the earth; i.e., $r = \theta/a_e$.

Furthermore, since we are interested in waves at large r from the source, we now make use of the asymptotic expansion for large arguments of $H_0^{(2)}(k_j r)$. Therefore, including the above approximation for curvature, our solution is

$$\{p_0\}_{A_j} = 2\pi a_s \frac{p_{as}}{\rho_s^0(D)} \frac{e^{(\chi_s - \lambda_s)a_s}}{(b_s + i\omega)^2} k_j \cdot \frac{[p_s(D)/p_0]_{H_j}}{[p_{n-1}/p_0]_{H_j}(\partial F_A/\partial k)_{\omega,j}} \left(\frac{r}{a_e \sin\theta}\right)^{1/2} \cdot \left(\frac{2}{\pi k_j r}\right)^{1/2} e^{i\omega(t - t_{as} - kr/\omega_j + \pi/4\omega)} \qquad (62)$$

From this form of the solution we see that our curvature correction factor

$$(r/a_e \sin\theta)^{1/2}$$

alters the amplitude in order to compensate for the effect of energy spreading over a spherical surface instead of a flat surface.

Barograph response and calibration. The type of microbarograph at Donnelley Seismological Laboratory has previously been described in the literature by *Ewing and Press* [1953] and *Donn et al.* [1954]. The frequency response of this instrument is given by

$$\mathcal{R}(\omega) = (1.35\omega)/[\{\omega^4 - \omega^2[\omega_F^2 + \omega_G^2 + 4\epsilon_F\epsilon_G(1 - \sigma^2)] + \omega_F^2\omega_G^2\}^2 + \{2\omega^3(\epsilon_F + \epsilon_G) - 2\omega(\omega_G^2\epsilon_F + \omega_F^2\epsilon_G)\}^2]^{1/2} \qquad (63)$$

$$\varphi_I = \tan^{-1}\left\{\frac{\omega^4 - \omega^2[\omega_F^2 + \omega_G^2 + 4\epsilon_F\epsilon_G(1 - \sigma^2)] + \omega_F^2\omega_G^2}{2\omega(\omega_G^2\epsilon_F + \omega_F^2\epsilon_G) - 2\omega^3(\epsilon_F + \epsilon_G)}\right\} - \pi$$

where $\mathcal{R}(\omega)e^{-i\varphi_I}$ is the barograph frequency response. The instrument constants are such that the galvanometer and float systems are critically damped, $\epsilon_F = \epsilon_G = 1$, and the coupling factor is negligible, $\sigma = 0$.

Barogram synthesis. For spherical boundary value problems with harmonic time dependence, the requirement that the solutions be periodic in θ causes ν to be an integer. This requirement by (60) restricts k_j to particular values, reducing our continuous (ω, k_j) phase spectrums for $F_A = 0$ to discrete points. For this problem, we use the continuous (ω, k_j) or (ω, c_j) curves when we integrate our solution over ω to obtain theoretical barograms. Using the continuous (ω, k_j) curves has been shown by *Weston* [1961] to be equivalent to keeping in the spherical solution only the terms which represent waves that have arrived at the detector without encircling the earth.

The flat-earth result given by (62) is obviously the wave which has come directly to the detector by way of the shortest route without passing the antipode. For reference purposes and to be consistent with other authors, we designate this arrival in the time domain as A_1. This solution is very similar in form to the result given by *Weston* [1961] for the spherical problem, assuming a flat-earth approximation. In fact, the θ or r dependence for spectral amplitude and phase are identical. The solution differs from ours in the manner of calculating the homogeneous solutions, the mode excitation, the source normalization, and the detail in modeling the atmosphere realistically. Moreover, he showed that for the A_2 arrival, which had traveled by way of the antipodal route, the spectral amplitude was the same as for the shorter route and had a phase corresponding to the longer route with a positive phase shift of $\pi/2$.

Since the derivation used here is for a horizontally stratified atmosphere with an approximate curvature correction, our solution cannot possibly give A_2. Therefore, using Weston's

result as a justification, we obtain the A_2 arrival by replacing r in the phase of (62) by r_2 and by adding a positive phase shift of $\pi/2$, where r_2 is given by

$$r_2 = a_s(2\pi - \theta) = 2\pi a_s - r \qquad (64)$$

Leaving the spectral amplitude the same for A_2 as for A_1, after A_2 has traveled a longer route, can be physically interpreted as a refocusing of the spectral energy at the antipode with a resultant shift in phase of $\pi/2$, which often occurs in problems involving a focus.

Integrating over ω so that the source used in the derivation of (62) has the observed pressure variation in the time domain, we have for A_1, from (62),

$$[p(r, 0; t)]_{Aj} \equiv [p_0]_{Aj} = \frac{1}{2\pi}\int_{-\infty}^{\infty} \{p_0\}_{Aj}\, d\omega$$

$$= \left(\frac{2}{\pi}\right)^{1/2} \frac{1}{(a_s \sin\theta)^{1/2}} \frac{e^{-\lambda_s a_s}}{\rho_s{}^0(D)}\, a_s p_{as}(I_1 + I_2) \qquad (65)$$

where

$$I_1 = \int_0^{\sigma_1} \mathfrak{F}_A{}^{(1)}(\omega) e^{i\omega(t-\tau_A)}\, d\omega + \int_{-\sigma_1}^{0} \mathfrak{F}_A{}^{(1)}(\omega) e^{i\omega(t-\tau_A)}\, d\omega$$

$$I_2 = \int_{\sigma_1}^{\infty} \mathfrak{F}_A{}^{(2)}(\omega) e^{i\omega(t-\tau_A')}\, d\omega + \int_{-\infty}^{-\sigma_1} \mathfrak{F}_A{}^{(2)}(\omega) e^{i\omega(t-\tau_A')}\, d\omega$$

$$\mathfrak{F}_A{}^{(1)}(\omega) = e^{\chi_s a_s} \frac{\mathbf{A}_{Aj}(\omega)}{(b_s{}^2 + \omega^2)} |k_j|^{1/2} \left[\frac{p_s(D)}{p_0}\right]_{Hj} = e^{\chi_s a_s} \mathfrak{F}_A{}^{(2)}(\omega) \qquad (66)$$

$$\mathbf{A}_{Aj}(\omega) = \{[p_{n-1}/p_0]_{Hj} (\partial F_A/\partial k)_{\omega,j}\}^{-1}$$

$$k_j/\omega = 1/c_j$$

$$\tau_A = t_{as} + r/c_j - \pi/4\,|\omega| + 2\theta_s/\omega$$

$$\theta_s = \tan^{-1}(\omega/b_s)$$

$$\tau_A' = \tau_A + \tau_\chi$$

$$\tau_\chi = -(a_s/\alpha_s)(\omega^2 - \sigma_1{}^2)^{1/2}/\omega$$

and where the phase velocity, c_j, and $[p_s(D)/p_0]_{Hj}\, \mathbf{A}_{Aj}(\omega)$ are even functions of ω. Thus from the criteria of (8) and the fact that $\omega(t - \tau_A)$ is odd about $\omega = 0$, we can calculate I_1 and I_2 from

$$I_1 = 2\int_0^{\sigma_1} \left[\frac{p_s(D)}{p_0}\right]_{Hj} \frac{\mathbf{A}_{Aj}(\omega)}{(b_s{}^2 + \omega^2)}\, k_j^{1/2} \cdot e^{(a_s/\alpha_s)(\sigma_1{}^2 - \omega^2)^{1/2}} \cos\omega[t - \tau_A]\, d\omega \qquad (67)$$

and

$$I_2 = 2\int_{\sigma_1}^{\infty} \left[\frac{p_s(D)}{p_0}\right]_{Hj} \frac{\mathbf{A}_{Aj}(\omega)}{(b_s{}^2 + \omega^2)}\, k_j^{1/2} \cdot \cos\omega[t - (\tau_A + \tau_\chi)]\, d\omega$$

For A_2 the above equations remain the same with the exception that τ_A is now given by

$$\tau_A = t_{as} + r_2/c_j - 3\pi/4\,|\omega| + 2\theta_s/\omega \qquad (68)$$

where r_2 is given by (64).

For the A_1 and A_2 barograms, we include the instrument response $\mathfrak{R}(\omega)$ and φ_I/ω given by (63).

Computational method. The theoretical barograms are calculated by means of two Fortran programs written for the IBM 7090 computer. The first is a modification of the air wave dispersion program described by *Press and Harkrider* [1962]. Its purpose is to calculate all the quantities in (67) which depend on layering alone. These quantities are $\mathbf{A}_{Aj}$, k_j, and the group velocity, $U_j = d\omega/dk_j$.

As in the original program, the initial step is to find the root, k_j, which satisfies $F_A = 0$ for a given input phase velocity, c_j. Once the root is determined by the computer, the homogeneous particle velocity and pressure ratios given by (56) are calculated at the midpoint in each layer.

Next, the root values of $\mathbf{A}_{Aj}$ and U_j are computed. To calculate $\mathbf{A}_{Aj}$, we need the value of $(\partial F_A/\partial k)_{\omega,j}$. We define a layer derivative matrix $(\partial a_m/\partial k)_\omega$, where

$$[(\partial a_m/\partial k)_\omega]_{lr} = [\partial(a_m)_{lr}/\partial k]_\omega \qquad (69)$$

is the definition of the lrth matrix element. From (69) and the definition of matrix multiplication, we see that the matrix $(\partial A_m/\partial k)_\omega$ can be given by the matrix products

$$(\partial A_m/\partial k)_\omega = (\partial a_m/\partial k)_\omega A_{m-1} + a_m(\partial A_{m-1}/\partial k)_\omega \qquad (70)$$

Therefore, using (70) and analytic expressions for (69) in each layer, starting from the surface layer, we can calculate the matrix $(\partial A/\partial k)_\omega$.

With the elements from this matrix, we compute $(\partial F_A/\partial k)_\omega$ from (41). Similiarly we calculate $(\partial F_A/\partial \omega)_k$ and form the group velocity U_j by the relation

$$U_i = -(\partial F_A/\partial k)_\omega/(\partial F_A/\partial \omega)_k \qquad (71)$$

As a check, we calculate a rough group velocity in two ways. The first is by numerical differentiation of the phase velocity. $\Delta c/\Delta k$ is obtained by perturbing c slightly and then finding a new k root. The second method is by numerical differentiation of F_A and using (71).

The purpose of the second program is to take the quantities calculated by the dispersion program and synthesize the pressure and barogram time variations at some surface detector. This is accomplished by applying the *Aki* [1960] approximation with linear amplitude intervals, an extension of an approximate evaluation of the integral

$$h(t) = 2\int_0^\infty A(\omega)\cos\omega[t - \tau(\omega)]\,d\omega \qquad (72)$$

where $A(\omega)$ is real in the frequency interval $\omega_1 < \omega_2$ and zero outside the interval. In Aki's evaluation it was also assumed that $A(\omega)$ was constant in this interval.

The first step in the evaluation is to divide the integration interval ω_1 to ω_2 into subintervals over which phase and amplitude are approximately linear in ω. With this approximation, (72) takes the form

$$h(t) = 2\sum_i \int_{\omega_i-\Delta\omega_i/2}^{\omega_i+\Delta\omega_i/2} A(\omega) \cdot\cos\varphi(\omega)\,d\omega \qquad (73)$$

where

$$A(\omega) = A_i + (\omega - \omega_i)(dA/d\omega)_i \equiv A_i + (\omega - \omega_i)a_i$$

$$\varphi(\omega) = \omega t - \omega\tau(\omega) = \varphi_i + (\omega - \omega_i)(d\varphi/d\omega)_i$$

with the i subscripted variables evaluated at the midpoint of the ith frequency interval $\Delta\omega_i$.

Defining t_g by $t_g = \tau + \omega\,(d\tau/d\omega)$, we see that

$$(d\varphi/d\omega)_i = \{t - [\tau + \omega(d\tau/d\omega)]\}_i \equiv t - t_{gi}$$

Thus, expanding cos φ in terms of these quantities and evaluating the resultant integral, we obtain the expression used in the Fourier synthesis program:

$$h(t) = 2\sum_i \left\{ A_i\Delta\omega_i \cos\omega_i(t - \tau_i) \cdot\frac{\sin[(\Delta\omega_i/2)(t - t_{gi})]}{(\Delta\omega_i/2)(t - t_{gi})} - \left(\frac{dA}{d\omega}\right)_i \Delta\omega_i \frac{\sin\omega_i(t - \tau_i)}{(t - t_{gi})} \cdot\left\{\frac{\sin[(\Delta\omega_i/2)(t - t_{gi})]}{(\Delta\omega_i/2)(t - t_{gi})} - \cos\left[\frac{\Delta\omega_i}{2}(t - t_{gi})\right]\right\}\right. \qquad (74)$$

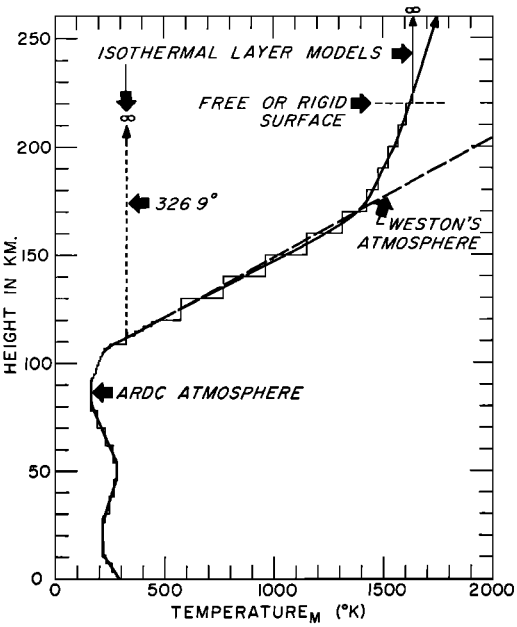

Fig. 1. ARDC standard atmosphere and its approximation by isothermal layers.

Discussion of frequency domain. The vertical temperature structure used to model the earth's atmosphere is the ARDC standard atmosphere (Figures 1 and 4) used by *Press and Harkrider* [1962]. This model was chosen because it was shown to explain adequately all the significant group-frequency arrivals in the observed barograms from the Soviet nuclear tests (Figures 2 and 3).

The ARDC standard model of the atmosphere has two temperature minimums, one at 18 km and the other at 85 km. For computation it is

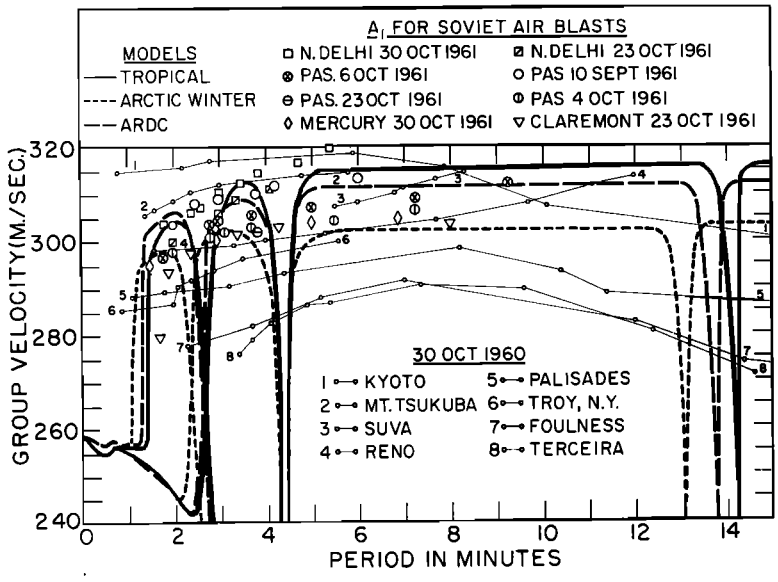

Fig. 2. Comparison of experimental group velocities for A_1 waves from Novaya Zemlya explosions with standard and extreme ARDC models. Data curves 1–8 from *Donn and Ewing* [1962].

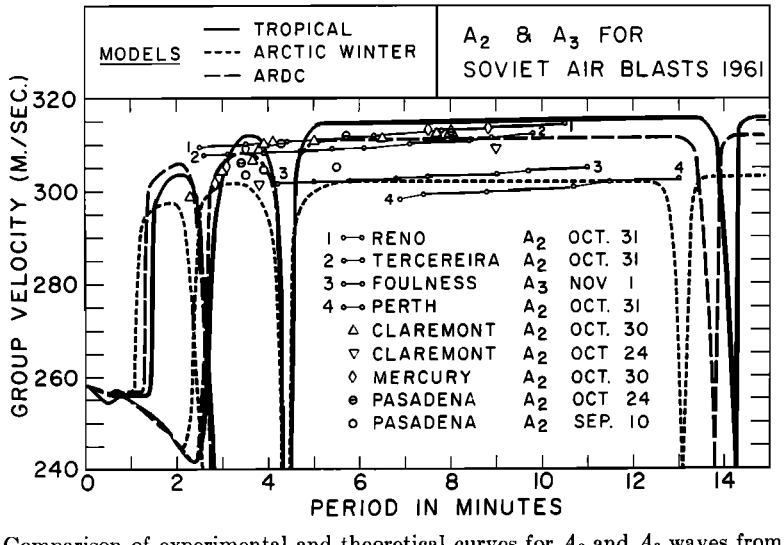

Fig. 3. Comparison of experimental and theoretical curves for A_2 and A_3 waves from Novaya Zemlya explosions. Data curves 1–4 from *Donn and Ewing* [1962].

represented by a digital model with 39 layers and is terminated with an isothermal half-space beginning at an elevation of 220 km.

The dispersion curves for this model are shown in Figures 5 and 6. A number of perturbations of this model were used by *Press and Harkrider* [1962] to determine the effect on dispersion due to digitization, the termination of the atmosphere, and the various parts of the atmospheric wave guide.

Press and Harkrider found that certain features of the dispersion curves were sensitive to particular regions of the vertical temperature and velocity structure. Their results concerning these dispersion effects may be summarized as follows: (1) The sequence of maximums or

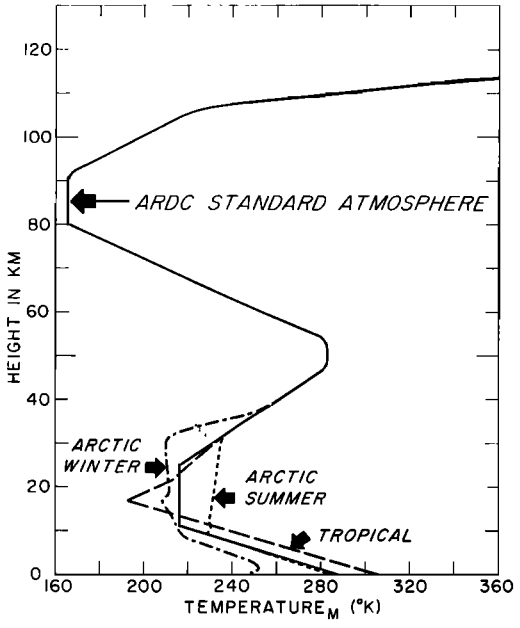

Fig. 4. Standard and extreme ARDC atmospheres.

plateaus in group velocity is sensitive to the properties of the lower 50 km of the atmosphere. In fact, recent work by *Pfeffer and Zarichny* [1963] indicates that the sequence of plateaus for the higher acoustic modes approaches the sound velocity of the lower wave guide. (2) The phase and group velocities of the acoustic modes approach the lowest velocity in the atmosphere at the high frequency limit. In our model this is the upper wave guide at 85 km; therefore the group velocity minimums are sensitive to the atmosphere above 50 km.

With the source theory presented in this paper it is possible to extend our investigation to the effect on amplitude. The effect of lower parts of the wave guide on spectral amplitude can best be seen in the following. From previous sections we know that the response of the medium to a surface source and receiver is given by $\mathbf{A}_A(\omega)$. The responses for S_2, S_1, S_0, GR_0, and GR_1 for the ARDC standard and arctic winter models are illustrated in Figure 7. The most striking feature is the similarity in shape between group velocity and amplitude. The similarity in shape demonstrates that the early-arriving waves are more efficiently excited by near-ground disturbances recorded by ground-based detectors than later arrivals which correspond to the group velocity minimums. This effect was predicted by *Press and Harkrider* [1962] on the grounds that early arrivals corresponding to the group velocity plateaus were controlled by the atmosphere structure below 50 km, whereas the group velocity minimums were sensitive to the atmosphere above 50 km.

Another interesting feature of the response curves is the secondary plateaus of S_2 and S_1 (shown as A and B in Figure 7) at frequencies corresponding to later long-period group arrivals. The secondary plateaus of S_2 and S_1 extend from a period of 2 and 3 minutes, respectively, to the long-period cutoff of each mode. For the S_2 mode this plateau for the late-arriving 2- to 3½-min wave yields an excitation equivalent to the earlier-arriving 1- to 1¼-min wave. The effect of terminating the model with a free surface instead of a half-space is to eliminate the hole in the spectrum near 14 min with a continuation of GR_0 at an amplitude equal to that shown for GR_1. A similar effect was shown for the group velocity plateau [*Press and Harkrider*, 1962]. Superimposed on the mode response curves is the amplitude response of the microbarograph with a peak amplitude of 0.0533 cm/μbar at a period of 1.6 min.

The effect of source and receiver height on spectral amplitude can be determined by the vertical distribution of the homogeneous pressure ratios. The distribution of this ratio as a function of period for two altitudes is given in Figure 8 for the ARDC standard model. The spectral amplitude is given by the product of $\mathbf{A}_A$ and the homogeneous pressure ratios at the source and receiver elevation. Thus a horizontal line in Figure 8 with a constant value less than 1 would indicate a uniform reduction in amplitude over surface amplitudes.

In Figure 8 we display the ratio for an altitude of 18.5 km, corresponding to the midpoint of the lower-velocity channel. In addition to an over-all reduction in amplitude relative to that of surface excitation, this ratio shows the following effects on amplitude. (1) There is very little change in the general shape of GR_0 and GR_1. The late-arriving waves for GR_1 are decreased slightly. The late-arriving GR_0 are increased slightly, especially at the short-period end. (2) The early-arriving waves for the acoustic modes corresponding to the group velocity plateaus show an increase in amplitude relative to the

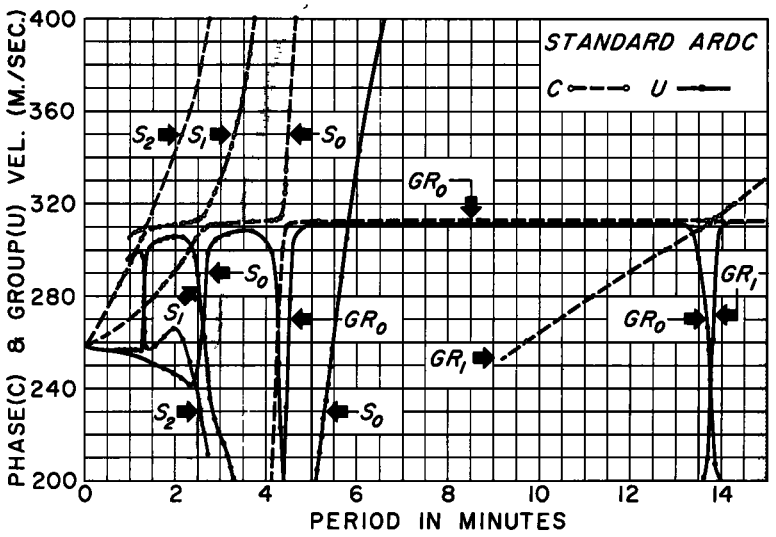

Fig. 5. Phase and group velocity dispersion curves for $S_{0,1,2}$ and $GR_{0,1}$ modes of ARDC standard atmosphere with half-space beginning at 220 km. Stippled region indicates where singular values of F occur. Cutoffs indicated by hatched region.

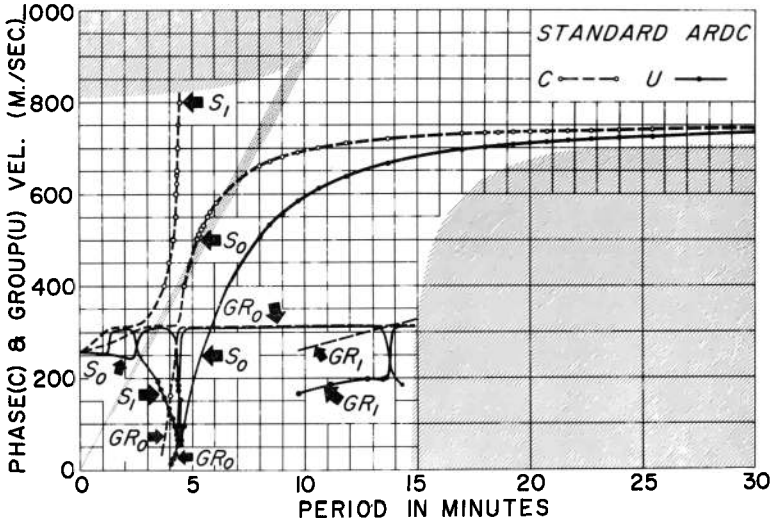

Fig. 6. Same as Figure 5 with different scale.

gravity modes. With either the source or detector at this altitude, the peak amplitudes of the S_2, S_1, and S_0 modes are equal to the peak amplitudes of the GR_0 and GR_1 modes. With both source and detector at this altitude (Figure 9), the peak amplitudes of the acoustic modes are greater than the gravity modes in the following order: $S_2 > S_1 > S_0$. (3) The secondary plateaus of S_2 and S_1 are reduced relative to the plateaus of early-arriving waves of all the modes. (4) The high-frequency late-arriving waves for the acoustic modes show an increase in excitation, and the long-period late-arriving waves for S_2 and S_1 show a decrease.

A detailed discussion of the amplitude or excitation effects of placing the source and receiver in the more interesting parts of the atmosphere is beyond the scope of this paper, partly because

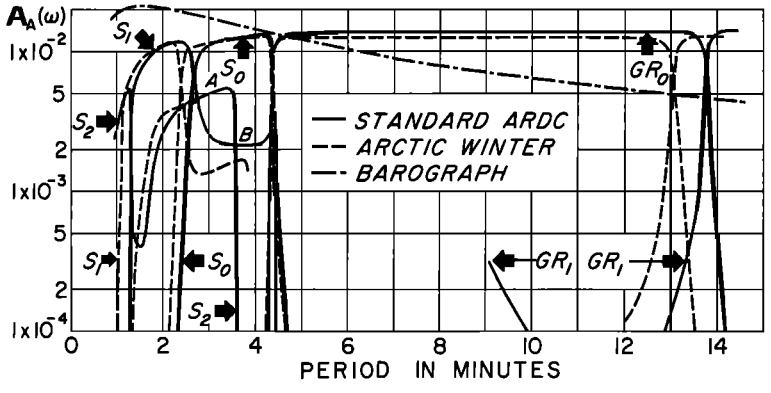

Fig. 7. Spectral amplitude of $A_A(\omega)$ for the ARDC standard and arctic winter atmospheres. Spectral amplitude of the barograph is superimposed.

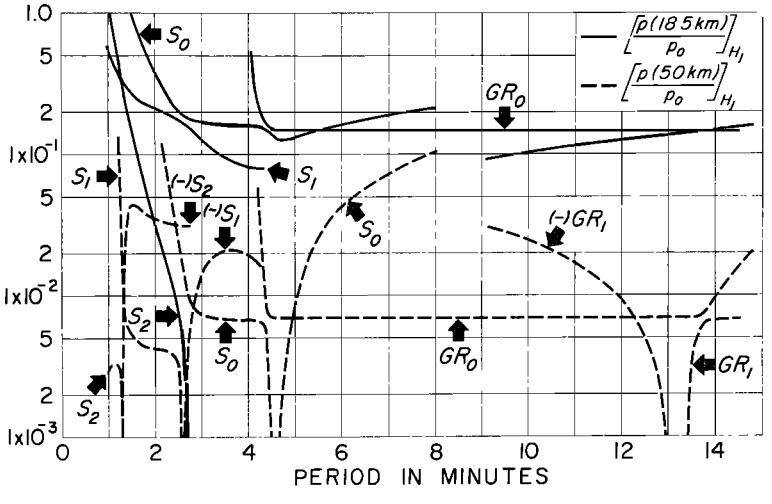

Fig. 8. Homogeneous pressure ratios at an altitude of 18.5 and 50 km for $S_{0,1,2}$ and $GR_{0,1}$ modes

the observed barograms used in this paper were produced by nuclear explosions at an altitude of less than 4 km.

The resultant spectral amplitudes displaying these effects are given in Figures 9, 10, 11, and 12 and can be summarized as follows: (1) In the lower velocity minimum, the gravity modes are comparatively unaffected as to shape. The excitation of the early-arriving waves for the acoustic modes are increased relative to early-arriving gravity waves. (2) In the relative velocity maximum between the minimums, the early-arriving acoustic waves are less excited than the corresponding gravity waves. (3) The effect of increasing altitude is to increase the excitation of the late-arriving waves relative to the early-arriving waves for each mode. For the short-period acoustic waves which travel near the acoustic velocity of the upper minimum, the relative increase in excitation is maximum in this channel, and the excitation of the long-period late arrivals continues to increase with altitude. The increase in relative excitation of the late-arriving portions of the GR modes with altitude is especially evident in Figure 12. At this altitude (125 km) the excitation plateaus for GR_1 and GR_0 have reversed their near-surface excitation roles; GR_1 now forms the short-period segment of the GR modes.

The majority of these results were postulated by *Press and Harkrider* [1962] from the manner in which different parts of the atmosphere af-

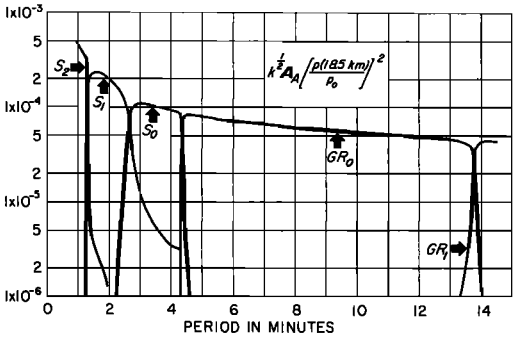

Fig. 9. Spectral amplitudes of $S_{0,1,2}$ and $GR_{0,1}$ modes for a source and receiver at an altitude of 18.5 km.

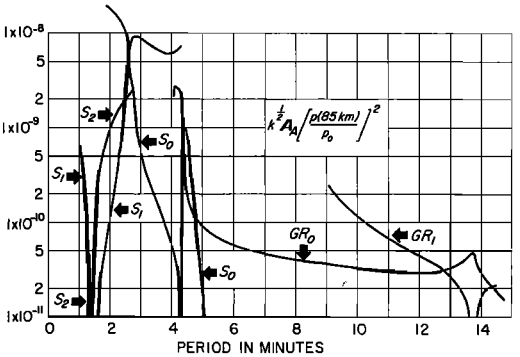

Fig. 11. Spectral amplitudes of $S_{0,1,2}$ and $GR_{0,1}$ modes for a source and receiver at an altitude of 85 km.

fected the dispersion results. Also, it must be remembered that these results hold for a 'white' source only. The effect of the scaling laws for nuclear weapons is such that some of these effects will not be apparent for theoretical barograms in the time domain. This effect will be discussed in greater detail later.

Discussion of time domain. To study the effect of source yield and altitude in the time domain under realistic bomb test conditions, we constructed theoretical barograms using the amplitude and dispersion results for the ARDC model, terminated by a half-space at 220 km. As a check on the conclusions drawn in the following paragraphs, selected barograms were made for an ARDC arctic winter model.

From seismic evidence, the approximate location of the Soviet tests gives a path of 8000 km for A_1 and an antipodal path of 3200 km for A_2 to the microbarograph at Donnelley Seismological Laboratory, Pasadena, California. The constants used for the bomb characteristics of a 1-kT explosion [*Glasstone*, 1962] are as follows: a peak excess pressure of 34.45 mb at a range of 1.61 km and a positive phase duration of 0.48 sec.

All theoretical barograms given in this section are on the same horizontal time scale and have a common fiducial time plotted at the left-hand margin of the figure. Since the plotting scale is determined internally by the program, the scales for various traces may differ even in the same figure. Therefore, in order to facilitate amplitude comparisons, we have indicated certain vertical amplitudes in the figures by means of numbers, arrows, and a horizontal dash at a peak and trough. The vertical scale for pressure waves is given in micro- or millibars of pressure and the vertical scale for barograms is given in centimeters of barograph recording.

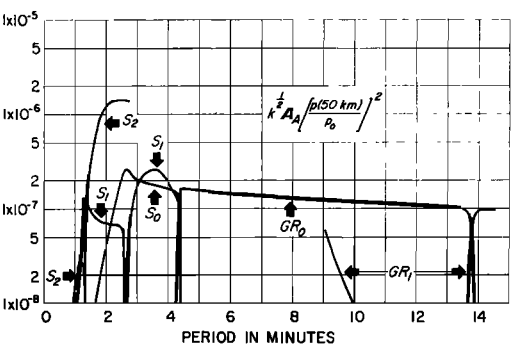

Fig. 10. Spectral amplitudes of $S_{0,1,2}$ and $GR_{0,1}$ modes for a source and receiver at an altitude of 50 km.

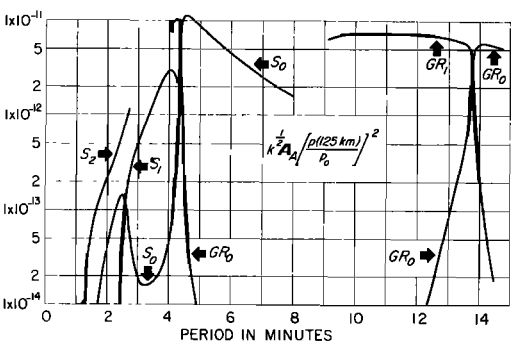

Fig. 12. Spectral amplitudes of $S_{0,1,2}$ and $GR_{0,1}$ modes for a source and receiver at an altitude of 125 km.

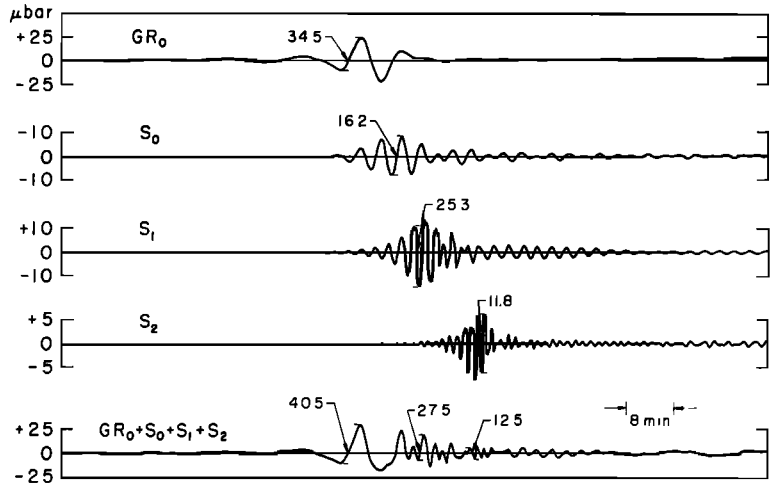

Fig. 13. Theoretical pressure variations of A_1 waves for the individual modes GR_0 and $S_{0,1,2}$. The fifth trace is the resultant wave for $GR_0 + S_0 + S_1 + S_2$.

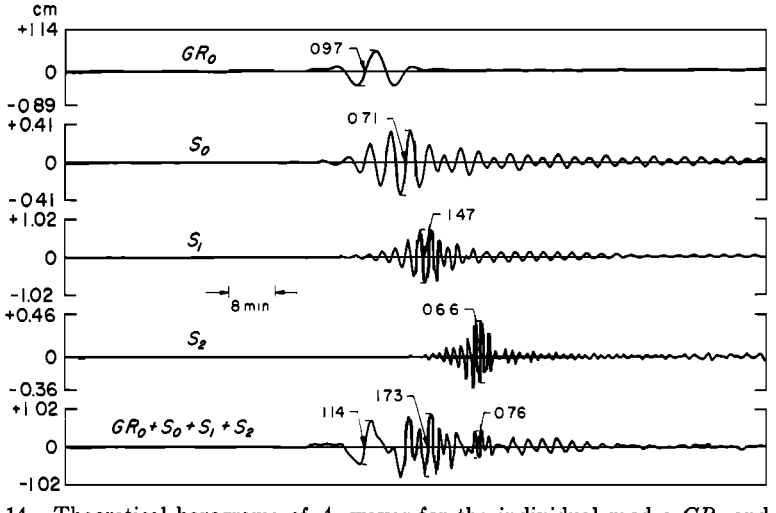

Fig. 14. Theoretical barograms of A_1 waves for the individual modes GR_0 and $S_{0,1,2}$. The fifth trace is the resultant wave for $GR_0 + S_0 + S_1 + S_2$.

The most significant features of the theoretical barogram for the ARDC standard and arctic winter models are given by the summation of five modes, S_2, S_1, S_0, GR_0, and GR_1. Of these, the least significant contribution was that of GR_1. In Figure 13 we show the theoretical pressure variation of A_1 for a 4-MT nuclear explosion at 2.13-km elevation. The first four traces are the individual modes GR_0, S_0, S_1, and S_2. The fifth trace is the summation of all the modes. It also contains GR_1, whose contribution is negligible. In Figure 14, we have the corresponding A_1 theoretical barograms for the same explosion. Comparison of Figures 13 and 14 demonstrates the response of the barograph to the pressure wave arriving at the detector. This response is seen in the relative increase in amplitude of the higher-frequency modes S_2, S_1, and S_0 to GR_0. In both figures we see that mode interference in the time domain significantly changes the character of the composite barogram. This is especially evident in the pressure variation, where the superposition of modes results in arrivals with spurious periods.

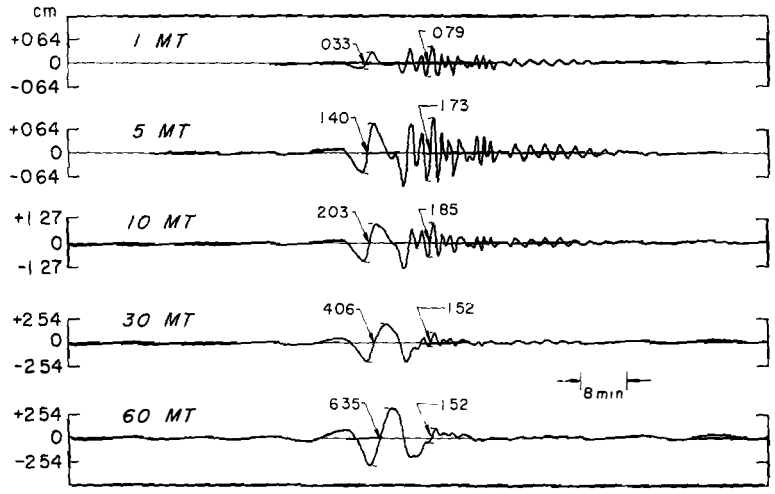

Fig 15. The effect of yield on theoretical barograms for A_1 waves.

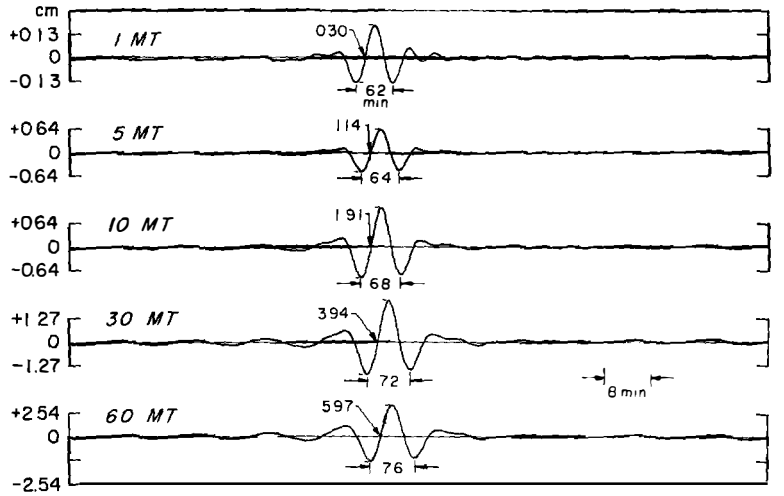

Fig. 16. The effect of yield on theoretical barograms of A_1 waves for the single mode GR_0.

For determining the effect of yield with source altitude constant, five barograms were synthesized for the following yields at an altitude of 2.13 km: 1, 5, 10, 30, and 60 MT (Figure 15). The most striking qualitative effect of increasing yield at the same source altitude, other than the obvious increase in amplitude, is the increase in the long-period part of the wave train relative to the shorter-period arrivals. This is especially noticeable in the extremes of the chosen yields. For 1-MT blasts the S_0 mode is the major mode, with S_1 and GR_0 almost equal to each other and somewhat less than S_0. For the 60-MT explosion the GR_0 mode is by far the largest, whereas S_0 is almost nonexistent and the S_1 contribution, although small, gives all of the high frequencies seen in the wave. This effect occurs despite the instrument response which accentuates the higher-frequency modes, S_0 and especially S_1.

From (68) we see that the only terms which could emphasize this mode with yield changes are the source terms in the spectral amplitude

$$[e^{(\alpha_s/\alpha_s)(\sigma_1^2-\omega^2)^{1/2}}]/(b_s^2+\omega^2)$$

for the long-period modes and $(b_s^2+\omega^2)^{-1}$ for the short-period modes, where σ_1 is the acoustic cutoff for the medium surrounding the source. Since $\sigma_1 = \lambda_s \alpha_s$ is independent of the yield, and

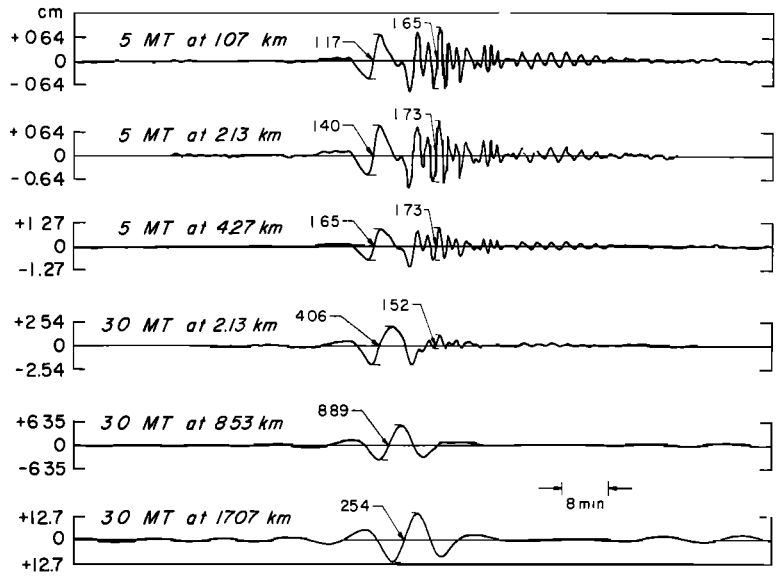

Fig. 17. The effect of altitude on theoretical barograms of A_1 waves.

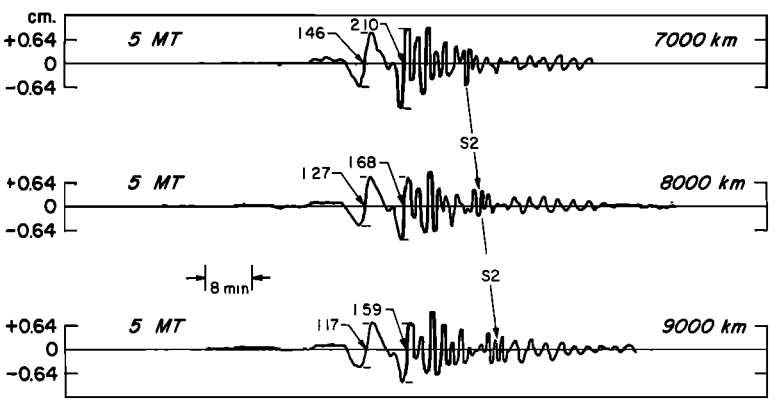

Fig. 18. The effect of distance on theoretical barograms of A_1 waves.

since by (12) and (13) a_s increases with yield, it is evident that the exponential term increases the relative excitation of the longer periods relative to the short periods with a yield increase. Similarly, b_s decreases with increasing yield and thus increases the spectral amplitude at long periods while decreasing the short periods. From these factors we see that the scaling laws induce a 'pseudo' nonlinearity to the problem. This is especially true for the time scale of the initial pressure variation as the bomb size increases. Figure 16 shows the increase in amplitude and fundamental period with increasing yield for A_1 barograms of a single mode, GR_0.

The effect of altitude for a constant yield is illustrated in Figure 17. For this purpose, we constructed three A_1 barograms for 5-MT explosions at altitudes of 1.07, 2.13, and 4.27 km. We made three additional A_1 barograms for 30-MT explosions at altitudes of 2.13, 8.53, and 17.07 km. With an increase of altitude from 1.07 to 4.27 km for a 5-MT bomb the barograms show an increase in amplitude of almost 50% in the part of the wave train corresponding to group arrival of GR_0. For a group arrival corresponding to S_1, the amplitude change is negligible. Both the over-all amplitude increase and the increase of the long waves relative to the

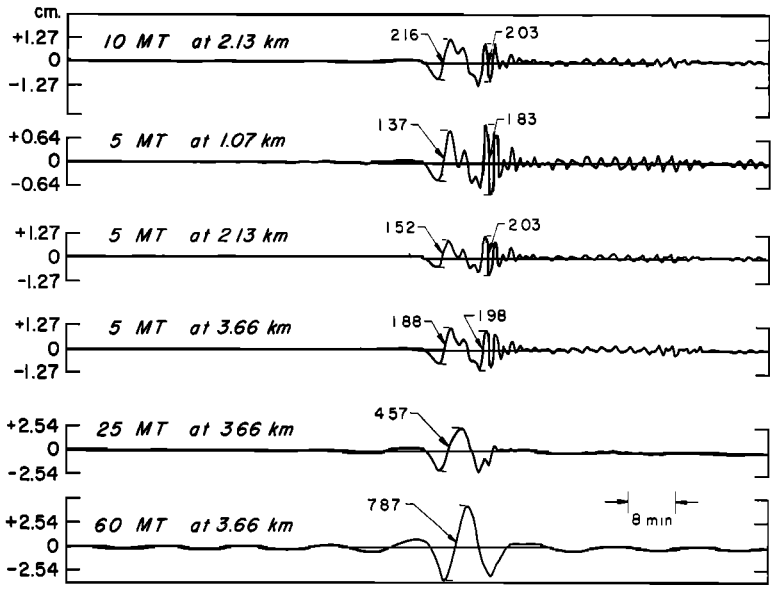

Fig. 19. The effect of yield and altitude on theoretical barograms of A_1 waves in an ARDC arctic winter atmosphere.

short waves with increasing altitude are due to the scaling laws used. This phenomenon is similar to the effect, discussed previously, of increasing the yield at constant altitude, since a_s increases and b_s decreases with an increase in either yield or altitude.

For the early-arriving short-period modes, such as S_1, the decrease in short period due to decreasing b_s is compensated in this altitude range by the inverse effect of the wave guide itself. In the discussion of frequency domain it was pointed out that in the part of the wave guide between the surface and the low-velocity channel the effect of increasing altitude is to increase the relative excitation of the acoustic modes relative to the longer-period *GR* modes.

For the 30-MT bombs, the increase in altitude shows an increase in the long-period arrivals and a decrease in the short-period arrivals. From an altitude of 8.53 to 17.07 km the short-period part of the train is negligible in amplitude. To demonstrate the effect of distance on the shape of the wave train in Figure 18, we calculated three barograms at distances of 7000, 8000, and 9000 km for a 5-MT bomb exploded at an altitude of 2.13 km. The wave train remains essentially the same for all three distances because the most predominant frequencies excited for a near-surface source and detector are the frequencies with almost constant phase and group velocity (Figures 7 and 5). The one noticeable difference is the migration of the S_2 mode through the wave train. This mode can be identified as a group or pocket of waves of about 1.2-min period which move toward the end of the wave train with increasing distance. The variation of amplitude with distance is discussed later.

Figure 19 shows A_1 barograms for an ARDC arctic winter atmosphere under various conditions of yield and bomb altitude. A comparison with theoretical barograms for the ARDC standard atmosphere yields the following observations: (1) The arctic winter wave train arrives at a later time than the ARDC standard corresponding to its lower group velocity plateaus. (2) The qualitative effects of varying yield and source altitude are the same as the ARDC standard model. (3) The major difference in the wave trains of the two atmospheres is caused by mode interference. This is due to the shift in phase for each mode caused by different phase velocities for the two models. (4) The amplitudes are essentially the same for the two models. Quantitative estimates of amplitudes for the composite barograms are complicated by mode interference.

Because of mode interference and the 'pseudo'

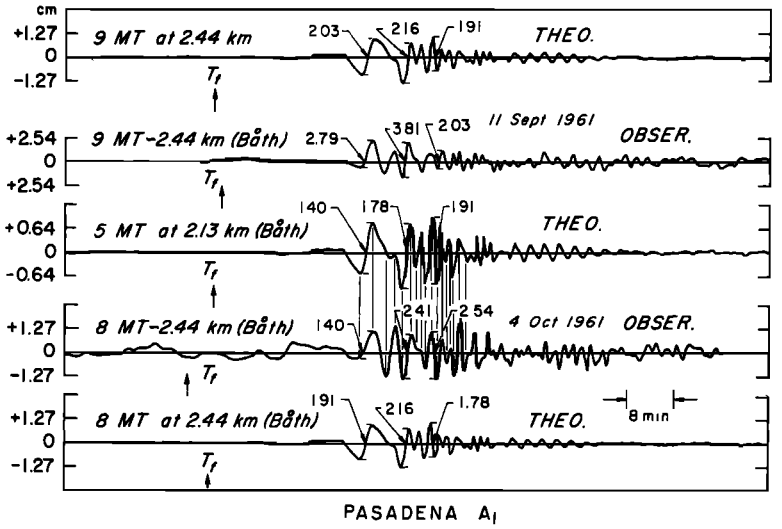

Fig. 20. Comparisons of theoretical and observed barograms of Pasadena A_1 waves, T_f arrows show common fiducial time.

nonlinearity induced by scaling laws, it is difficult to recover bomb yield and altitude from measurements on an observed or experimental barogram. Another method of attack is to compare observed barograms with theoretical barograms constructed from estimates of approximate yield and altitude.

Comparison of theoretical and observed barograms. In this section theoretical barograms are compared with observed barograms produced at various stations by the Soviet nuclear explosions in Novaya Zemlya during the fall of 1961. The yields of the explosions are taken from the reported seismic estimations given by *Båth* [1962]. The altitudes for the 60-MT explosion on October 30 and the 25-MT explosion on October 23 were reported in the newspapers as being at 12,000 feet or 3.66 km. Båth classified the altitudes as low, intermediate, and high for the 1961 explosions, the October 23 and 30 explosion being classified as high. With this in mind I have arbitrarily assigned the following altitudes to Båth's qualitative estimates: 3.66 km for high-altitude explosions, 2.44 km for intermediate-altitude explosions, and 1.22 km for low-altitude explosions.

In Figures 20 to 26 the theoretical and experimental records have been aligned on the time scale for the best fit. The arrows indicate where a fiducial time would fall on each record.

In Figure 20 the first two traces are the theoretical and observed recordings of A_1 waves from a 9-MT explosion at 2.44 km on September 10. In comparing the records we see that there is good agreement in phase, group, and amplitude except in the region corresponding to the S_0 group arrival. In this region, between the numbers 2.03 and 2.16 on the theoretical trace, we have a slight phase shift, and mode interference causes a spurious long period. On the observed trace the $3\frac{1}{2}$-min S_0 arrival is well developed. In this figure and in Figures 21 and 22, the S_0 arrival is distorted, whereas on the observed records the arrival is well developed. The relative excitation between early group arrivals is consistent on both traces.

The last two traces are the observed and theoretical recordings of A_1 waves from an 8-MT explosion at 2.44 km on October 4. The over-all amplitudes agree fairly well. There is a disagreement in the relative excitation of the early group arrivals. On comparing the observed barogram with the theoretical recording of A_1 for 5 MT at 2.134 km, the third trace in this figure, a much better fit in relative excitation can be seen.

In Figure 21 the first two traces are the theoretical and observed recordings of A_1 for 11 MT at 2.44 km on October 6. The third and fourth traces are the theoretical and observed recordings respectively for 5 MT at 1.22 km on October 20. The theoretical and observed records for both explosions show reasonably good agree-

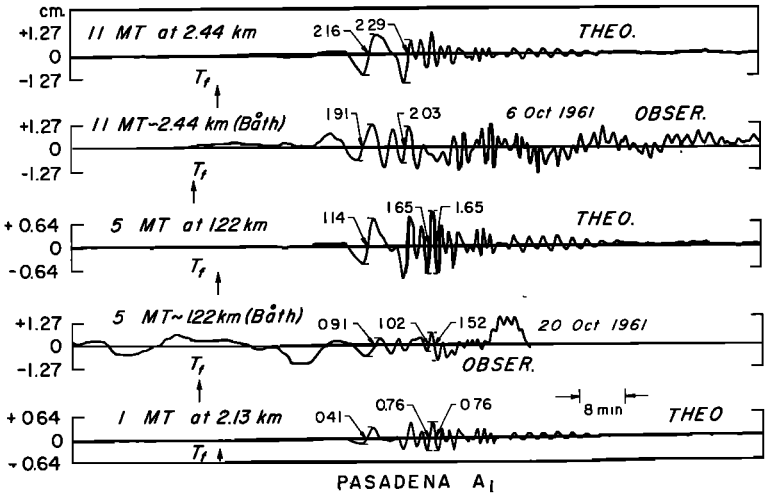

Fig. 21. Comparisons of theoretical and observed barograms of Pasadena A_1 waves. T_f arrows show common fiducial time.

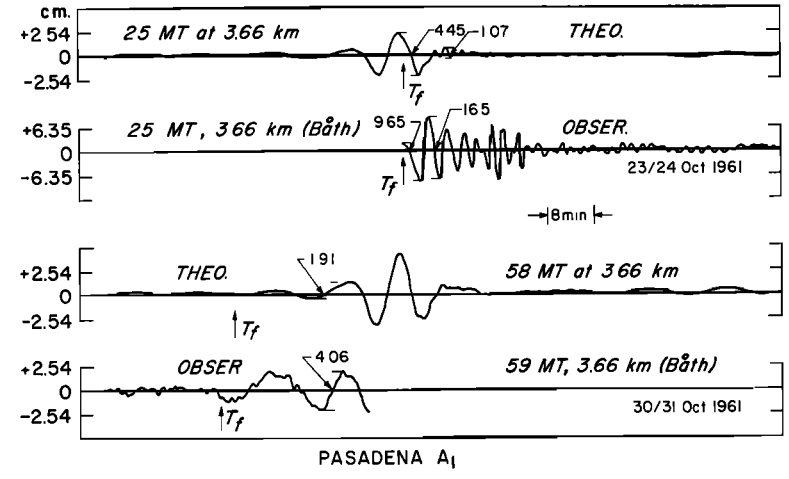

Fig. 22. Comparisons of theoretical and observed barograms of Pasadena A_1 waves. T_f arrows show common fiducial time.

ment in over-all amplitude of the early part of the wave train. The fifth trace is a theoretical recording of A_1 for an explosion of 1 MT at 2.13 km. The bomb yield and elevation were chosen so as to match the S_1 amplitude with the recorded amplitude for the October 20 explosion. This change in yield and altitude reduces the amplitude of the long-period component at the beginning of the wave train relative to S_1.

In the previous comparisons of theoretical and observed A_1 recordings, there is a major discrepancy. The observed recording shows a late-arriving wave train of an almost constant period of from 1 to 2 min. This train is not found on the theoretical barograms. From the dispersion curves in Figure 5 this arrival could well be the steep part of the group velocity curves of S_2 and S_1 which coincide at about $1\frac{1}{4}$. The part at the far right of the record might correspond to the relative maximum in group velocity of 268 m/sec at a period of 2 min for the S_2 mode. This late arrival would correspond to the secondary plateau in amplitude for S_2.

There were no complete A_1 recordings at Pasadena for the large explosions of October 23 and 30. In Figure 22 the first two traces are the

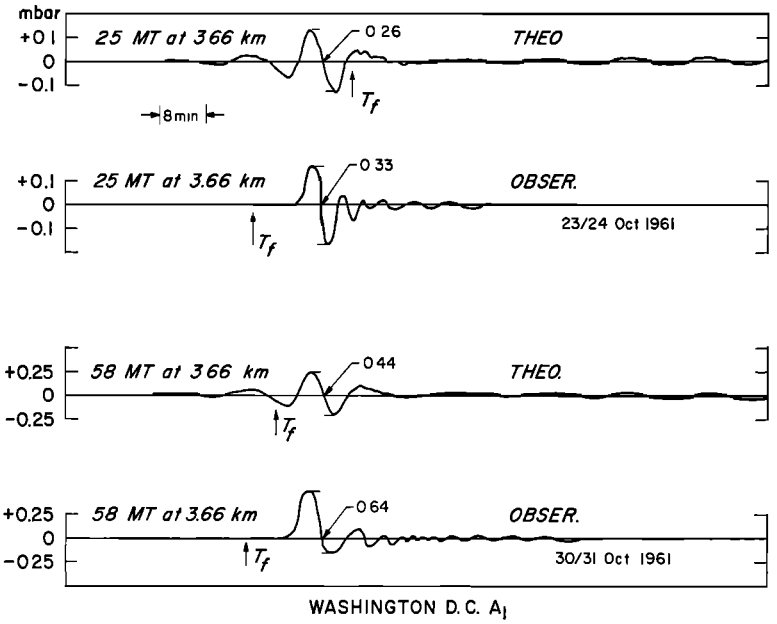

Fig. 23. Comparisons of theoretical and observed barograms of Washington, D. C., A_1 waves. T_f arrows show common fiducial time.

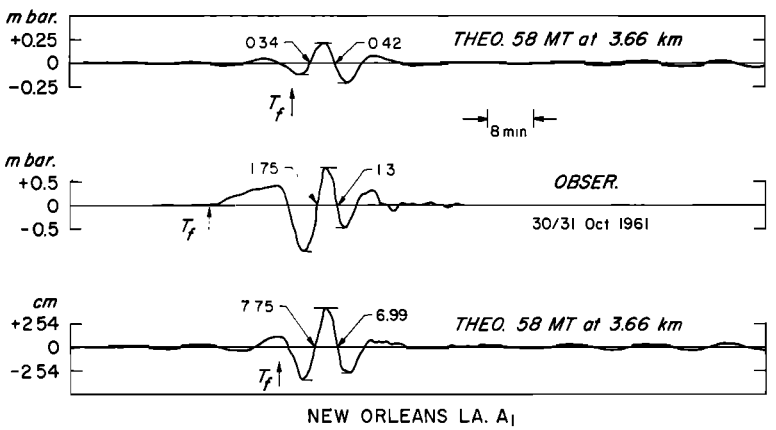

Fig. 24. Comparisons of theoretical and observed barograms of New Orleans, La., A_1 waves. T_f arrows show common fiducial time.

theoretical and the incomplete part of the observed A_1 recording for the 25-MT explosion at 3.66 km on October 23. The last two traces are the incomplete observed A_1 and the theoretical barograms for October 30. If the assumed alignment is correct, we see that the theoretical amplitudes are down by a factor of about 2 for the predominant long-period arrival and by a factor of at least 10 for the later-arriving high frequencies.

For a more complete study of the A_1 recordings on October 23 and 30, 1961, we use some barograms recorded at two meteorological stations [*Wexler and Hass*, 1962]. In Figure 23, theoretical pressure waves for the large explosions are compared with the observed A_1 records for Washington, D. C. The absolute amplitudes are in fair agreement; the shape agreement is poor. This is especially true for the long-period arrivals at the onset of the wave. The difference

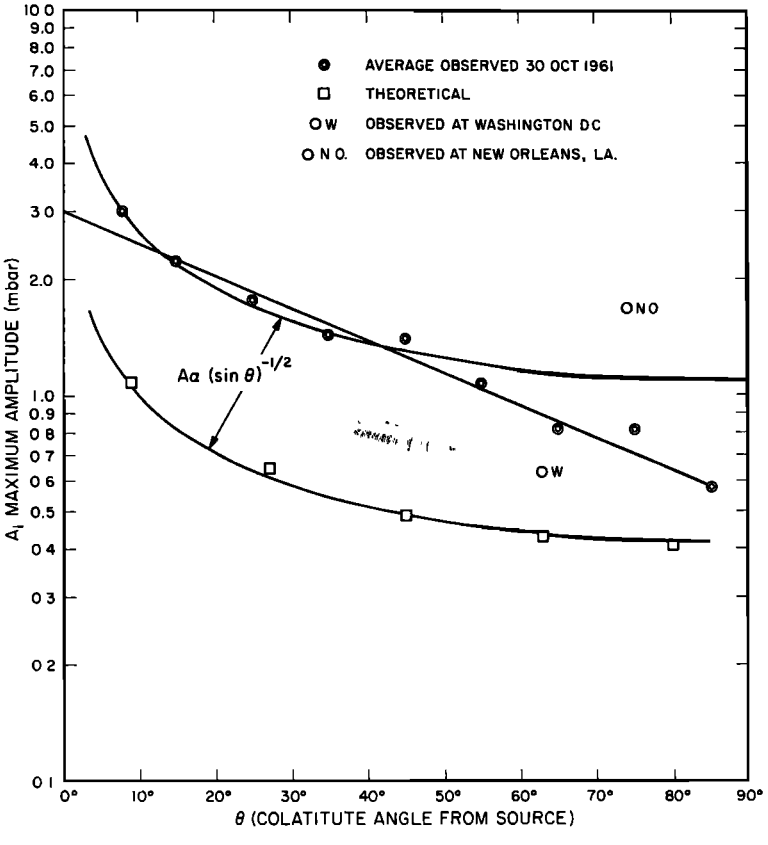

Fig. 25. Variation of theoretical and observed maximum amplitudes of A_1 with colatitude from source for a 58-MT explosion.

in shape appears to be due to the recording instrument response, which, for Washington, was assumed to be flat and without phase distortion. Evidence supporting this argument can be seen by comparing Figures 24 and 23. The middle trace in Figure 24 and the last trace in Figure 23 are the A_1 recordings of the same event on October 30 at the New Orleans and Washington stations, respectively. Although the recording instruments are similar and the source distances comparable, their shapes are very dissimilar. In fact there is good agreement in shape and character for the observed A_1 at New Orleans and the theoretical pressure arrival shown as the top trace in Figure 24. If the theoretical pressure wave is recorded by an instrument with the same response as the Pasadena microbarograph, we obtain the theoretical A_1 barogram given by the bottom trace in Figure 24. The resultant agreement in phase, group, and relative amplitude between the observed and theoretical arrivals is outstanding. The poor theoretical agreement in absolute amplitude at New Orleans and the fair agreement at Washington are misleading, as we shall see.

Figure 25 shows the A_1 meteorological data collected by *Wexler and Hass* [1962] for the October 30 explosion. Maximum amplitudes from the weather stations were averaged for 10° intervals, measured from the source. From (66), the amplitudes should primarily vary with colatitude as $(\sin \theta)^{-1/2}$. The effect of dispersion on amplitude is slight because of the almost constant group velocity for GR_0, the dominant mode. That the effect of dispersion is indeed negligible can be seen in the plotted maximum amplitudes obtained from theoretical pressure time records for a bomb of 58 MT. Fitting a $(\sin \theta)^{-1/2}$ curve to the observed data, we obtain an excellent fit out to 45°, a distance of 5000 km.

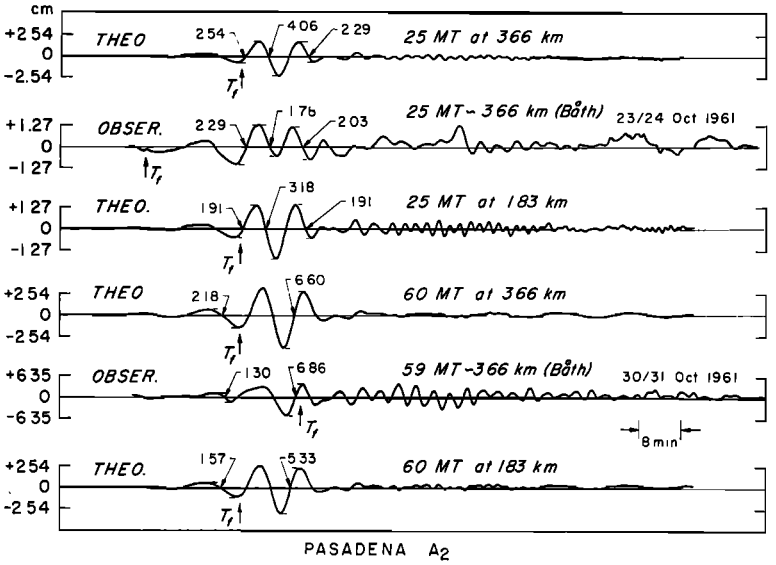

Fig. 26. Comparison of theoretical and observed barograms of Pasadena, Calif., A_2 waves. T_f arrows show common fiducial time.

Comparing this curve with that of the theoretical pressure waves indicates that the scaling law for the large explosions yields a result that is 50% less than observed values.

The deviation of the averaged observed values from the geometric factor at angles greater than 45° is probably due to the internal friction of the atmosphere. Also shown in the figure are the maximum amplitudes for the individual stations of Washington and New Orleans. Their departure from the exponential distance function for the averaged observations beyond 45° can be traced to the meteorological conditions along the individual travel paths, such as high-altitude winds [*Wexler and Hass*, 1962]. This scaling-law-induced discrepancy for large explosions is also evident in the theoretical and observed comparisons for the A_2 arrivals. *Donn and Ewing* [1962] observed that the A_2 arrival is down 50% from the A_1 arrival at distances comparable to that to Pasadena for the October 30 event. Theoretical barograms for A_1 and A_2 yield essentially the same amplitudes because of the slight dispersion for the dominant mode and because internal friction in the equations of motion is neglected. Therefore the effect of not considering internal friction over the long travel path of A_2 is compensated by the 50% underscaling of the theoretical barograms, and a close amplitude agreement for the theoretical and observed A_2 arrivals at Pasadena is obtained.

Theoretical and observed recordings for A_2 are shown in Figure 26. These records are for the large explosions on October 23 and 30. For the 25-MT explosion shown in the two top traces the agreement in phase, group, and amplitude is excellent for the early-arriving waves. For the 60-MT explosion shown in the third and fourth traces the agreement is still good. The distortion in period between the numbers 1.30 and 6.86 on the observed record appears to be due to some sort of interference.

The differences in arrival times between the theoretical and observed A_1 and A_2 records leads, at most, to discrepancies in times of 3%. The discrepancy in relative excitation between the acoustic modes and gravity modes for large yields and altitudes is also felt to be due to the scaling laws, which are probably not valid for large yields and high altitudes.

Conclusions. 1. The major features on the barogram can be explained by the superposition of four modes, S_0, S_1, S_2, and GR_0.

2. Different parts of the vertical temperature structure of the atmosphere control the excitation of these modes. The zone with a velocity minimum near 20 km controls the early-arriving acoustic modes. The region with a velocity maxi-

mum at about 50 km controls the early-arriving gravity modes. The minimum velocity region at about 85 km controls the short-period acoustic modes which travel at a group velocity equal to the acoustic velocity of this channel. The upper atmosphere controls the late-arriving long-period waves of each mode.

3. A scaled point source is sufficient to model thermonuclear explosions.

4. The observed shift in dominance of certain frequencies with yield and altitude can generally be explained by means of the empirical scaling laws derived from the direct wave near the explosion.

5. Mode interference in the time domain and the 'pseudo' nonlinearity induced by scaling laws make it difficult to determine bomb yield and altitude from observed barograms. If elevation is known, rough estimates of yield can be obtained with this theory.

6. The internal friction of the atmosphere is negligible for polar path lengths up to 50°. Even for path lengths up to 80° the frictional effect can be masked by meteorological conditions encountered along individual great-circle paths.

7. For large yields and high altitudes the scaling laws seem to overemphasize the long-period gravity arrivals relative to the short-period acoustic arrivals. Also the scaling laws appear to underestimate the peak amplitude of the large explosions by as much as 50%. Some changes in scaling laws are thus indicated for these large events, a result which does not surprise us in view of the use of low-yield data in deriving these laws.

Acknowledgments. I am grateful to Professor Frank Press for his support and encouragement throughout this study. Many valuable discussions were held with Drs. D. L. Anderson and C. B. Archambeau. Their cooperation and support are acknowledged with gratitude.

This research was supported by contract AF-49 (638)-1337 of the Air Force Office of Scientific Research as part of the Advanced Research Projects Agency project Vela.

References

Aki, K., Study of earthquake mechanism by a method of phase equalization applied to Rayleigh and Love waves, *J. Geophys. Res., 65,* 729–740, 1960.

Båth, M., Seismic records of explosions—especially nuclear explosions, 3, *Forsvarets Forskningsanstalt Avdel., 4,* A4270–4721, 1962.

Carpenter, E. W., G. Harwood, and T. Whiteside, Microbarograph records from the Russian large nuclear explosions, *Nature, 189*(4805), 847, 1961.

Donn, W. L., and M. Ewing, Atmospheric waves from nuclear explosions, *J. Geophys. Res., 67,* 1855–1866, 1962*a*.

Donn, W. L., and M. Ewing, Atmospheric waves from nuclear explosions, 2, The Soviet test of October 30, 1961, *J. Atmospheric Sci., 19,* 264–273, 1962*b*.

Donn, W., R. Rommer, F. Press, and M. Ewing, Atmospheric oscillations and related synoptic patterns, *Bull. Am. Meteorol. Soc., 35,* 301–309, 1954.

Erdelyi, A., W. Magnus, F. Oberhettinger, and F. Tricomi, *Tables of Integral Transforms, 2,* 9, 1954.

Ewing, M., and F. Press, Further study of atmospheric pressure fluctuations recorded on seismographs, *Trans. Am. Geophys. Union, 34,* 95–100, 1953.

Glasstone, S., *The Effects of Nuclear Weapons,* U. S. Government Printing Office, Washington 25, D. C., 1962.

Haskell, N. A., The dispersion of surface waves on multilayered media, *Bull. Seismol. Soc. Am., 43,* 17–34, 1953.

Hunt, J. N., R. Palmer, and Sir William Penney, Atmospheric waves caused by large explosions, *Phil. Trans. Roy. Soc. London, A., 252,* 275–315, 1960.

Lamb, H., *Hydrodynamics,* Dover Publications, New York, 1945.

Pekeris, C. L., The propagation of a pulse in the atmosphere, 2, *Phys. Rev., 73,* 145–154, 1948.

Pfeffer, R. L., and J. Zarichny, Acoustic gravity wave propagation from nuclear explosions in the earth's atmosphere, *J. Atmospheric Sci., 19,* 256–263, 1962.

Pfeffer, R. L., and J. Zarichny, Acoustic gravity wave propagation in an atmosphere with two sound channels, *Geofis. Pura Appl., 55,* 175–199, 1963.

Press, F., and D. Harkrider, Propagation of acoustic-gravity waves in the atmosphere, *J. Geophys. Res., 67,* 3889–3908, 1962.

Rose, G., J. Oksman, and E. Kataja, Round-the-world sound waves produced by the nuclear explosion on October 30, 1961, and their effect on the ionosphere at Sodankylä, *Nature, 192*(4808), 1173–1174, 1961.

Scorer, R. S., The dispersion of a pressure pulse in the atmosphere, *Proc. Roy. Soc. London, A, 201,* 137–157, 1950.

Szegö, G., Über einige asymptotische entwicklungen der Legendreschen funktionen, *Proc. London Math. Soc., 36,* 427–450, 1933.

Wares, G. W., K. W. Champion, H. L. Pond, and A. E. Cole, Model atmospheres, in *Handbook of Geophysics,* 1-1–1-37, The Macmillan Company, New York, 1960.

Weston, V. H., Pressure pulse received due to an explosion in the atmosphere at an arbitrary alti-

tude, 1, *Univ. Mich. Radiation Lab. Rept. 2886-I-T*, 1960.

Weston, V. H., The pressure pulse produced by a large explosion in the atmosphere, *Can. J. Phys., 39*, 993, 1009, 1961*a*.

Weston, V. H., The pressure pulse produced by a large explosion in the atmosphere, 2, *Univ. Mich. Radiation Lab. Contract Rept. AF 19 (60A) 5470*, 1961*b*.

Weston, V. H., Intermediate results for thermosphere model, *Univ. Mich. Radiation Lab. Mem. 2886-521-M*, 1961*c*.

Wexler, H., and W. A. Hass, Global atmospheric pressure effects of the October 30, 1961, explosion, *J. Geophys. Res., 67*, 3875–3887, 1962.

Yamomoto, R., The microbarographic oscillations produced by the explosions of hydrogen bombs in the Marshall Islands, *Bull. Am. Meteorol. Soc., 37*, 406–409, 1956.

Yamomoto, R., A dynamical theory of the microbarographic oscillations produced by the explosions of hydrogen bombs, *J. Meteorol. Soc. Japan, 35*, 32–40, 1957.

(Manuscript received August 14, 1964.)